Optical depth of the Universe to ultrahigh energy cosmic ray scattering in the magnetized large scale structure

Kumiko Kotera* and Martin Lemoine+

Institut d'Astrophysique de Paris UMR7095 - CNRS, Université Pierre & Marie Curie, 98 bis boulevard Arago F-75014 Paris, France

(Received 17 January 2008; published 12 June 2008)

This paper provides an analytical description of the transport of ultrahigh energy cosmic rays in an inhomogeneously magnetized intergalactic medium. The latter is modeled as a collection of magnetized scattering centers, such as radio cocoons, magnetized galactic winds, clusters or magnetized filaments of large scale structure, with negligible magnetic fields in between. Magnetic deflection is no longer a continuous process, it is rather dominated by scattering events. We study the interaction between high-energy cosmic rays and the scattering agents. We then compute the optical depth of the Universe to cosmic ray scattering and discuss the phenomenological consequences for various source scenarios. For typical parameters of the scattering centers, the optical depth is greater than unity at 5×10^{19} eV, but the total angular deflection is smaller than unity. One important consequence of this scenario is the possibility that the last scattering center encountered by a cosmic ray be mistaken with the source of this cosmic ray. In particular, we suggest that part of the correlation recently reported by the Pierre Auger Observatory may be affected by such delusion: this experiment may be observing in part the last scattering surface of ultrahigh energy cosmic rays rather than their source population. Since the optical depth falls rapidly with increasing energy, one should probe the arrival directions of the highest energy events beyond 10^{20} eV on an event by event basis to circumvent this effect.

DOI: 10.1103/PhysRevD.77.123003 PACS numbers: 98.70.Sa, 98.65.Dx

I. INTRODUCTION

The problem of the origin of ultrahigh energy cosmic rays has generally been expressed as the conjunction of two questions: (i) how can particles be accelerated to energies in excess of 10^{20} eV? (ii) why is the source not seen in the arrival directions of the highest energy events? Progress on the former question has certainly been hindered by our relative lack of knowledge on acceleration mechanisms and high energy processes in the most powerful astrophysical objects. Regarding the latter question, progress has been mostly limited by the scarcity of experimental data at the highest energies, at least until very recently.

Indeed, the first results of the Pierre Auger Observatory, which have just been published, report a significant correlation of the arrival directions of the highest energy events with a catalog of active galactic nuclei (AGN) closer than 75 Mpc [1,2]. This observation certainly marks an important step in the search for the source of ultrahigh energy cosmic rays. However, one should not over interpret the significance of these results. In particular, the likelihood of the reported coincidence rests on the comparison with isotropic arrival directions, yet the large-scale structure is known to be highly inhomogeneous at least up to 75 Mpc. Since AGN are known to cluster with the large-scale structure, one cannot exclude at present that the observed correlation remains a coincidence if the source itself clusters with the large-scale structure [2]. More will be said on these data in Sec. IV of the present paper.

Furthermore, there exist other (and sometimes contradictory) claims in the literature on the existence of correlations of ultrahigh energy cosmic ray arrival directions with various source catalogs [3], the strongest being the association with BL Lacertae objects reported in Refs. [4–6] (see also Refs. [7,8]). Since the existing data is so scarce at the highest energies, the assessment of the statistical significance remains a difficult task. Finally, the reported evidence for multiplets of events tends to suggest that the source lies in the arrival direction of the events clusters. However, some of these clusters show interacting galaxies as the sole peculiar objects on the line of sight [9], while a more recent multiplet appears correlated with interacting clusters of galaxies [10,11]. Taken at face value, all these claims do not allow to draw a clear and consistent picture of the source of ultrahigh energy cosmic rays.

It is admitted that cosmic magnetic fields must play a key role in this puzzle, although which role exactly is also a question that is still seeking for an answer. And this source of uncertainty is in turn related to our poor knowledge of the strength and the distribution of extragalactic magnetic fields (see Refs. [12,13] for detailed reviews of existing data). There exists a rather large body of literature on the relation between cosmic magnetic fields and ultrahigh energy cosmic rays. Most studies have constructed models of extragalactic magnetic fields and then resorted to Monte Carlo simulations in order to quantify the influence of these fields on the time, energy, and angular images expected in large scale detectors. One must, however,

*kotera@iap.fr
+lemoine@iap.fr

underline the analytical works of Refs. [14,15] on cosmic ray transport in tangled extragalactic magnetic fields of homogeneous power, those of Refs. [16,17], which discuss the particular effect of magnetic lensing, and finally Refs. [18–20], which discuss diffusive transport in a magnetized supercluster.

Earlier numerical studies have addressed the phenomenology of ultrahigh energy proton propagation in tangled magnetic fields of homogeneous power [21–28]. There has since been a trend toward more realistic magnetic field configurations. For instance, Refs. [29–34] have studied the diffusive or nondiffusive propagation in a magnetized local supercluster, and Ref. [35] has brought to light the spectral distortions induced by the interaction of ultrahigh energy cosmic rays with a supercluster harboring large scale regular magnetic fields. More recently, several studies have attempted to model a realistic configuration in which the magnetic field follows the matter density and then studied the transport of ultrahigh energy cosmic rays in the resulting structure. In order to construct the magnetic field, Refs. [36–42] have used numerical simulations of large scale structure formation involving a passive magnetic field whose strength was normalized to the value measured in clusters of galaxies. References [43–46] have rather reconstructed the extragalactic magnetic field by scaling the field strength to the underlying density field.

In general, these studies have assumed the magnetic field to be all pervading (albeit, with a more or less pronounced degree of inhomogeneity) so that magnetic deflection has been modeled as a continuous process. This assumption has been relaxed in Ref. [47], which provides numerical simulations of cosmic ray arrival directions after scattering with fossils of radio-galaxy lobes. Similarly, Ref. [48] has mentioned the possibility of discrete cosmic ray interactions with localized regions of enhanced magnetic fields, their discussion pointing toward clusters of galaxies as the main scattering agents.

This picture in which ultrahigh energy cosmic ray transport occurs through random discrete events is indeed more likely to be valid on distance scales up to a few hundreds of Mpc as a consequence of the high degree of clustering of matter in the Universe. For instance, even if the magnetic field were produced in a uniform manner at high redshift (see Ref. [49] for a review of models of the origin of large scale magnetic fields), then the present-day magnetic field should be highly inhomogeneous, as a result of the amplification of the magnetic field in the shear and compressive flows associated with the formation of nonlinear structures [40,41,45,50,51] (see also [52] for a general discussion). In these simulations, voids in the large scale structure are essentially deprived of magnetic field.

Furthermore, if one attributes the origin of the extragalactic magnetic field to pollution by a subclass of galaxies, for instance, starburst galaxies [53–55] or radio galaxies [56–58], the magnetic field configuration should resemble that of a percolating process (see Ref. [59] for a clear illustration). As explained further below, if the filling factor of the polluted regions becomes comparable to that of the filaments of large scale structure, the filaments themselves become the scattering agents as in Refs. [40,41,45,51].

The goal of the present paper is to provide an analytical description of ultrahigh energy cosmic ray transport in such an inhomogeneous medium, which is modeled by scattering centers embedded in an unmagnetized intergalactic medium.

These scattering centers comprise the filaments just as the clusters of galaxies but also all possible regions of locally enhanced magnetic fields, such as galactic winds, groups of galaxies, large scale structure shocks, and fossil radio-galaxy cocoons. One motivation of the present work is thus to make progress toward a more realistic magnetic field configuration, which takes into account those localized regions of intense magnetic activity. In order to do so, we first sketch a census of relevant scattering centers (Sec. II) then analyze their respective influence.

The present work is further motivated by the fact that Refs. [40,41,45,51] diverge as to the conclusions they draw on the influence of the extragalactic magnetic fields on ultrahigh energy cosmic rays, even though they try to construct *ab initio* predictions for the distribution of these large scale magnetic fields. This difference stems from the uncertainty on the origin of these magnetic fields, notwithstanding the complexity of modeling accurately the evolution of magnetic fields in the formation of large scale structure. Analytical tools become useful in this context, as they allow to parametrize the influence of such magnetic fields on the images and spectra of ultrahigh energy cosmic rays. This in turn will help to deconvolve this effect from existing and upcoming data, and therefore to infer useful constraints on these magnetic fields.

In the present description, magnetic deflection is no longer a continuous process, but is instead dominated by scattering events. We thus use the notion of the optical depth of the Universe to ultrahigh energy cosmic ray scattering and discuss the phenomenological consequences. In particular, we show that the optical depth decreases very abruptly as the energy increases, because the source distance scale decreases due to increasing energy losses, and because the influence of cosmic magnetic fields diminishes with increasing energy.

We argue that the energy beyond which the Universe becomes translucent or transparent to cosmic ray scattering may be tantalizingly close to the threshold beyond which experiments search for counterparts $E \simeq 4$–6×10^{19} eV. This could have profound consequences for our interpretation of existing data. For instance, if most sources lie beyond the last scattering surface, one could mistake the scattering centers on the last scattering surface (such as starbursts, old radio galaxies, or giant shock waves) with the source of ultrahigh energy cosmic rays.

The phenomenological consequences thus differ widely from the case of continuous deflection in an all-pervading medium. We thus discuss in some detail the expected effects and their relation to current and future observations of cosmic ray arrival directions.

This paper is laid out as follows. In Sec. II, we sketch a census of possible scattering centers and their influence on the optical depth of the Universe to cosmic ray scattering. We also calculate the distance to the last scattering surface and compare it with the expected source distance scale. In Sec. III, we discuss the transport of cosmic rays in this strongly inhomogeneous medium and the expected observational consequences. We notably provide sky maps of the expected optical depth up to different distances for our local universe. Finally, in Sec. IV, we summarize our findings and comment on the existing data in the framework of the present model. The physics of the interaction of cosmic rays with scattering centers is discussed in the appendix.

II. THE OPTICAL DEPTH OF THE UNIVERSE TO HIGH-ENERGY COSMIC RAY SCATTERING

A. Scattering centers in the large scale structure

We adopt a description in which the extragalactic magnetic field is inhomogeneous. If this magnetic field originates from a subclass of galaxies, its configuration is bound to follow that of the large scale structure, since the mixing length in the Universe is small for cosmological standards: for typical intergalactic velocities of $\sim$300 km/s, the length traveled in a Hubble time is only $\simeq 4$ Mpc. Note that the mixing length is even less in filaments, for which the typical dispersion of velocities is of order 50 km/s.

Obviously, at a given energy, the total optical depth to cosmic ray scattering is dominated by the structures with the largest $n\sigma$, where n represents the space density and σ the cross-section of the magnetized halo. One should thus focus on the radio halos of radio galaxies, the magnetized winds of star-forming galaxies, and on larger scales to clusters of galaxies and filaments as well as their surrounding accretion shock waves.

1. Radio halos

Radio halos of old radio galaxies (deemed radio ghosts) have been already considered as possible sites of ultrahigh energy cosmic ray scattering in Ref. [47]. This study evaluates their space density as $n_{\rm rg} \simeq 10^{-2}$–$10^{-1}$ Mpc^{-3}, the radius of their magnetized halos as $r_{\rm rg} \sim 0.5$–1 Mpc and their magnetic field $B_{\rm rg} \sim 1$ μG. Such quasar outflows have also been examined in detail in Ref. [57] as a site of magnetic pollution of the intergalactic medium, but their results differ from those above. These latter authors find a much lower magnetic field strength $B_{\rm rg} \sim 10^{-9}$ G, and to a substantially larger extent, $r_{\rm rg} \simeq$ 1–5 Mpc, for a comparable space density. With respect to the results of Ref. [57], the scattering should be dominated by the subpopulation of recently formed quasars (at redshifts $z \lesssim 4$), which have $r_{\rm rg} \sim 2$–4 Mpc and $B_{\rm rg} \sim 3 \times 10^{-9}$ G. The main difference between these calculations results from the different modeling of the bubble evolution. The former study assumes that the bubble settles in pressure equilibrium in a rather dense and hot intergalactic environment (with $\rho/\langle\rho\rangle \sim 30$ and $T \simeq 10^8$ K), while the latter argues that the bubble expands until its velocity matches that of the Hubble flow and takes the surrounding intergalactic medium (IGM) to be much colder and less dense ($T \sim 10^4$ K and $\rho/\langle\rho\rangle = 1$). Both fix the magnetic strength to lie at a fraction of equipartition with thermal energy, although this fraction to equipartition $\epsilon_B = 0.5$ in Ref. [47] and $\epsilon_B = 0.1$ in Ref. [57]; furthermore, Ref. [57] adopts ϵ_B as the equipartition fraction before expansion of the bubble, assuming that the magnetic field then decays with expansion. This study thus neglects all possible further amplification mechanisms of B; hence, their estimate (at a given ϵ_B) should be considered as a lower limit. If one instead considers ϵ_B as the equipartition fraction of the magnetic field at present, the magnetic field strength inside the bubble can be related to the kinetic energy of the outflow and the size of the bubble as follows:

$$B_{\rm rg} = 5 \times 10^{-8}\ {\rm G} \left(\frac{\epsilon_B}{0.1}\right)^{1/2} \left(\frac{E_{\rm rg}}{10^{59}\ {\rm ergs}}\right)^{1/2} \left(\frac{r_{\rm rg}}{1\ {\rm Mpc}}\right)^{-3/2}. \quad (1)$$

This latter estimate agrees with the conclusions of Ref. [58], which studies the degree of magnetization of the IGM by radio-galaxy jets and lobes. The outflow energy 10^{59} ergs is an average energy for a quasar population [47]: it corresponds to a black hole mass $M_{\rm BH} \simeq 3 \times 10^7 M_\odot$, radiating $L_{\rm bol} \simeq 3 \times 10^{45}$ ergs/s over 10^7 yrs [57]. Note however that the observational compilation of Ref. [60] leads to slightly higher values for $E_{\rm rg}$ and $B_{\rm rg}$. These authors have observed that the lobes of 70% of field radio galaxies in their sample have a much higher energy content $\sim 10^{60}$–10^{61} ergs than the remaining 30% in clusters (about 10^{58} ergs), with a typical volume $V \sim$ 0.03–0.3 Mpc^3 and inferred minimum energy magnetic field strengths in the range 3–30 μG. If the magnetic field is to decay as $V^{2/3}$ during the subsequent expansion of these bubbles, the final value for $B_{\rm rg}$ would be of order 0.1 μG for a typical radius $r_{\rm rg} \simeq 3$ Mpc, as above. In the following, we thus consider the possible range of values $B_{\rm rg} = 1$–10×10^{-8} G and typical radius $r_{\rm rg} \simeq$ 1–3 Mpc.

Finally, Refs. [47,57] estimate the space density of quasar outflows from the observed density of quasars at high redshifts and the typical duration of the quasar phase (taken as 10^7 yrs). Their estimate of $\sim 10^{-2}$–10^{-1} Mpc^{-3} agrees with the recent determinations of the black hole number density at low redshifts, in particular $n(>10^7 M_\odot) \simeq 2$–$4 \times 10^{-2}$ Mpc^{-3} [61], although Ref. [62] reports a number density that is smaller by about an order

of magnitude. In what follows, we thus consider the range $n_{\rm rg} = 3 \times 10^{-3} - 3 \times 10^{-2}$ Mpc^{-3}.

2. Magnetized galactic winds

Galactic winds have been proposed as a source of magnetic pollution of the intergalactic medium by various authors, see in particular [53–55]. Such outflows have been observed in different galaxies, for instance in the starbursting nearby dwarf galaxy M82 with wind speed $v \simeq 2000$ km/s and extension $\sim$10 kpc [63], or in massive star-forming Lyman break galaxies at high redshifts with wind speed $v \sim 1000$ km/s and extending as far as hundreds of kpc [64], maybe up to $\simeq 1$ Mpc [65] (see Ref. [66] for a review).

Galactic winds are also a key ingredient for theoretical models, which attempt explaining the metal enrichment of the intergalactic medium [59,67–69]. At the present time, it is not clear which galaxy type (if any) dominates the pollution. Starburst dwarf galaxies appear more akin at producing large winds, however, they also have a smaller gaseous content and a smaller energetic reservoir. In the following, we use the most recent simulations of Ref. [59], which detail the properties of galactic winds. This study shows that the number of wind-blowing galaxies is relatively insensitive to the stellar mass of the parent galaxy in the range $10^8 M_\odot \lesssim M_* \lesssim 10^{10} M_\odot$ as a result of the opposed influences of wind ram pressure and amount of infalling material, and that this number falls at both ends of this mass range. At $z \simeq 0$ and in this mass range, the typical wind radius increases slowly with galaxy mass as follows: $r_{\rm gw} \simeq 200$ kpc for $M_* = 10^8 M_\odot$, $r_{\rm gw} \simeq 800$ kpc for $M_* = 10^9 M_\odot$, and $r_{\rm gw} \simeq 1$ Mpc for $M_* = 10^{10} M_\odot$. Overall, the contribution $n_{\rm gw} r_{\rm gw}^2$ will be dominated by dwarf galaxies of stellar mass $M_* \sim 10^9 M_\odot$. The number density $n_{\rm gw}$ of galaxies surrounded by a wind at $z = 0$ can be derived from the filling factor $f_{\rm gw}$ of the winds; unfortunately, this quantity appears to depend strongly on the model, taking values between 2×10^{-2} and unity. The median value corresponds to $f_{\rm gw} = 0.1$–0.2, which gives a density $n_{\rm gw} \simeq f_{\rm gw}/V_{\rm gw} \simeq 2. - 5 \times 10^{-2}$ Mpc^{-3}, with $V_{\rm gw} = (4\pi/3) r_{\rm gw}^3$ the wind volume. Note that this number is comparable to the number density of galaxies of stellar mass above 10^8–$10^9 M_\odot$. If the filling factor becomes substantially larger, the galactic winds will overfill the filaments in which they reside; therefore, the filaments themselves become the scattering centers.

Concerning the strength of $B_{\rm gw}$, Ref. [55] indicates that most winds have a magnetic field with $B_{\rm gw} \simeq 10^{-8}$–$10^{-7}$ G at $z = 0$, the range covering conservative and optimistic assumptions concerning the amplification of $B_{\rm gw}$. Such amplification may have been detected in the outflow of M82, where a magnetic field strength as high as 10 μG [70] has been reported in the first 10 kpc. Ref. [54] has argued that the magnetic field could be amplified through the Kelvin-Helmholtz instability during ejection.

3. Clusters of galaxies

Clusters of galaxies are rare structures in the Universe, $n_{\rm cg} \simeq 10^{-5} h_{70}^3$ Mpc^{-3}, but they are known to host strong magnetic fields, with $B_{\rm cg|c} \sim 1$–10 μG in the innermost radius $r_{\rm cg|c} \sim 100$ kpc [12,71]. Measurements of the magnetic field in the cluster outskirts are rather scarce as a result of the smaller electron density and magnetic field strength. The minimum energy interpretation of recent synchrotron data nevertheless indicates that $B_{\rm cg} \sim 1$ μG out to $r_{\rm cg} \sim 1$ Mpc [72]. Theoretical expectations tend to differ. For instance, Ref. [40] shows that B varies with cluster mass, and indicates that for a massive cluster $B_{\rm cg} \sim 1$ μG within $r_{\rm cg} \simeq 0.2$ Mpc, then falls to $B_{\rm cg} \sim 10^{-7}$ G within $r_{\rm cg} \simeq 1$ Mpc, $B_{\rm cg} \sim 10^{-8}$ G within $r_{\rm cg} \simeq 2$ Mpc, and finally $B_{\rm cg} \sim 10^{-9}$ G within $r_{\rm cg} \simeq 4$–5 Mpc, while Fig. 5 of Ref. [73] indicates more extended magnetic fields, with $B_{\rm cg} \sim 1$ μG within $r_{\rm cg} \simeq 1$ Mpc, then falls to $B_{\rm cg} \sim 10^{-7}$ G within $r_{\rm cg} \simeq 3$ Mpc, $B_{\rm cg} \sim 10^{-8}$ G within $r_{\rm cg} \simeq 4$ Mpc, and finally $B_{\rm cg} \sim 10^{-9}$ G within $r_{\rm cg} \simeq 5$ Mpc. In the following, we take these two limits as a range for $B_{\rm cg}$ and $r_{\rm cg}$.

Note that about half of galaxies lie outside of clusters; hence, one can treat clusters of galaxies and the above field radio ghosts and field galactic winds as distinct scattering centers.

4. Filaments and walls of large scale structure

Filaments or walls of large scale structure are not expected to be sources of magnetic pollution *per se*. However, they may be pervaded with an average magnetic field produced in the accretion shocks surrounding them or generated in and ejected by the galaxies they contain, provided the filling factor of the resulting magnetic pollution in the filament/wall volume is of order unity. In the following, we will consider both possibilities.

If, as before, the magnetic energy density in the filament/wall is a fraction ϵ_B of the thermal energy of the IGM, one infers a magnetic field strength

$$B_{\rm f} = 3.5 \times 10^{-8}\ {\rm G} \left(\frac{\epsilon_B}{0.1}\right)^{1/2} \left(\frac{\rho_{\rm f}}{10\langle\rho_{\rm b}\rangle}\right)^{1/2} \left(\frac{T_{\rm f}}{10^6\ {\rm K}}\right)^{1/2}, \quad (2)$$

$\rho_{\rm f}$ and $T_{\rm f}$ denoting the filament baryonic density and temperature.

The typical length scale of a filament is $l_{\rm f} \sim 15$ Mpc, its radius $r_{\rm f} \sim 1$–2 Mpc, and the typical separation between two filaments $d_{\rm f} \sim 25$ Mpc [74].

During the formation of nonlinear structures, shock waves develop as a consequence of the infall of material on filaments, walls, and clusters of galaxies. Numerical simulations indicate that the typical radius of external shock waves around filament it is of the order of $r_{\rm sh} \simeq 2$–3 Mpc [75,76]; the typical velocity of these shock waves is of order $v_{\rm sh} \sim 300$–1000 km/s. Such shock waves have been proposed a site of magnetic field amplification (see for instance [77]) and cosmic ray acceleration [78–80].

If the magnetic field in the shock wave vicinity corresponds to a fraction of equipartition with the shock energy density $\rho v_{\rm sh}^2$, one finds

$$B_{\rm sh} \simeq 10^{-7}\ {\rm G}\left(\frac{\epsilon_B}{0.1}\right)^{1/2}\left(\frac{\rho_{\rm ext}}{\langle\rho_{\rm b}\rangle}\right)^{1/2}\left(\frac{v_{\rm sh}}{1000\ {\rm km/s}}\right)^{1/2}. \quad (3)$$

Note that $\rho_{\rm ext}$ refers to the density of infalling material. The estimate $\epsilon_B \sim 0.1$ gives the right order of magnitude for the inferred value of magnetic field strength $\sim 100\ \mu$G in young supernovae remnants assuming a typical interstellar medium density and comparable shock speed [81,82].

If cosmic shock waves amplify the magnetic field up to the value $B_{\rm sh}$ given above, one should then expect the filament to be endowed with a significant fraction of $B_{\rm sh}$ out to the shock radius. In effect, the amount of matter accreted through the shock in a Hubble time in units of the quantity of matter contained inside the structure at the present time can be expressed as

$$f_{\rm acc} \simeq \frac{\rho_{\rm ext}}{\rho_{\rm in}}\frac{v_{\rm sh}H_0^{-1}}{r_{\rm f}} \sim 0.3\left(\frac{v_{\rm sh}}{1000\ {\rm km/s}}\right)\left(\frac{r_{\rm f}}{2\ {\rm Mpc}}\right)^{-1} \times\left(\frac{\rho_{\rm f}}{10\langle\rho_{\rm b}\rangle}\right)^{-1}. \quad (4)$$

Note that the estimate $B_{\rm f}$ given in Eq. (2) agrees with that of $B_{\rm sh}$ to within a factor of a few (even though it was derived through other means).

B. Optical depth and last scattering surface for cosmic ray scattering

Depending on the strength of the magnetic field in a halo and its coherence length, the interaction of a particle may either lead to diffusion inside the structure, at sufficiently low energy, or to a weak deflection angle, at higher energies. The details of the interaction between a particle and a magnetized structure is described in detail in the appendix.

Homogeneously distributed scattering centers

Out of simplicity, we first assume that the scattering centers are distributed homogeneously in the Universe with a typical mean free path to interaction d_i, where i refers to the type of scattering center (e.g. magnetized galactic wind, radio halo, filament ...). We will discuss in Sec. II C the influence of inhomogeneity on the conclusions of the discussion that follows. For scattering centers of density n_i and cross-section σ_i, $d_i = (n_i\sigma_i)^{-1}$. The mean free path to interaction with any scattering center is written as $\bar{d}$:

$$\bar{d} = \frac{1}{\sum_i n_i\sigma_i}. \quad (5)$$

The optical depth to ultrahigh energy cosmic ray scattering over a path length l is then defined as

$$\tau = \frac{l}{\bar{d}} = l\sum_i n_{\rm i}\sigma_i. \quad (6)$$

To make concrete estimates, assume that one type of scattering center dominates, with typical interaction length d_i:

$$\tau \simeq 3.1\left(\frac{l}{100\ {\rm Mpc}}\right)\left(\frac{d_i}{32\ {\rm Mpc}}\right)^{-1}. \quad (7)$$

The above fiducial value $d_i = 32$ Mpc corresponds to spherical scattering centers of density $n_i = 10^{-2}\ {\rm Mpc}^{-3}$ and radius $r_i = 1$ Mpc; however, it is also a typical value for the interaction distance to filaments of the large scale structure.

The above optical depth characterizes the number of scatterings along a path length l, but it does not provide information on the angular spread of the cosmic ray image on the detector. Hence, it is useful to introduce an effective optical depth $\tau_{\rm eff}$, which becomes unity when the path length l is such that the particle has suffered a deflection of order unity. If at each scattering, the squared deflection is noted $\delta\theta_i^2$, then the number of scatterings to achieve a deflection of order unity reads $1/\delta\theta_i^2$. The scattering length $l_{\rm scatt}$ of cosmic rays in the medium, which corresponds to the distance over which the deflection becomes of order unity, can be written as

$$l_{\rm scatt} = \frac{1}{\sum_i n_i\sigma_i\delta\theta_i^2}. \quad (8)$$

We thus define the effective optical depth $\tau_{\rm eff}$ as

$$\tau_{\rm eff} = \frac{l}{l_{\rm scatt}} = l\sum_i n_{\rm i}\sigma_i\delta\theta_i^2. \quad (9)$$

The angular deflection can be expressed in a simple way as a function of the Larmor radius $r_{{\rm L}|i}$ of the particle in structure i, of the magnetic field coherence length λ_i of this structure, and of the characteristic path length $\bar{r}_i$ through the structure, which amounts to $(\pi/2)r_{\rm s}$ for a sphere of radius $r_{\rm s}$ or $(\pi/2)^2 r_{\rm f}$ for a filament of radius $r_{\rm f}$ (see also the appendix). Using the formula provided in the appendix [in particular Eq. (A3)], one can rewrite the effective optical depth as

$$\tau_{\rm eff} \simeq l\sum_i n_{\rm i}\sigma_i\left(1 + \frac{2r_{{\rm L}|i}^2}{\bar{r}_i\lambda_i}\right)^{-1}. \quad (10)$$

Obviously, one always has $\tau_{\rm eff} < \tau$. One should interpret the two optical depths as follows: $\tau < 1$ (which implies $\tau_{\rm eff} < 1$) means that the Universe is transparent to cosmic ray scattering on the scale l, while $\tau > \tau_{\rm eff} > 1$ means that the Universe is opaque over this scale, i.e. the accumulated angular deflection is greater than unity. The intermediate regime, $\tau > 1 > \tau_{\rm eff}$ is interesting; it corresponds to a translucent situation in which cosmic rays suffer one to

many scatterings but the accumulated angular deflection remains smaller than unity.

The phenomenology of the cosmic ray signal on the detector then depends on the typical source distance, which should be used for l, as well as on the characteristics of the scattering agents described above. Assuming rectilinear propagation of the particles, the source distance scale is of order $l_{\rm max}$, the maximal distance that a particle of energy E can travel without losing its energy. Indeed, if the source population is continuously emitting and homogeneous (the latter being a good approximation on scales beyond a few hundred Mpc), the flux $F(<l)$ received from sources located within a distance l increases as l

$$F(<l) = n_{\rm s}\dot{N}_{\rm UHECR} l, \tag{11}$$

where $n_{\rm s}$ denotes the source density and $\dot{N}_{\rm UHECR}$ the number of cosmic rays emitted by a source per unit time. In the case of bursting sources, one finds the same scaling (see Ref. [14])

$$F(<l) = \dot{n}_{\rm s} N_{\rm UHECR} l. \tag{12}$$

In this equation, $\dot{n}_{\rm s}$ should now be understood as the rate of bursting sources per unit time and unit volume, and $N_{\rm UHECR}$ as the total number of cosmic rays emitted by a source.

Hence, in both cases, most of the flux comes from sources located at distance of order $l_{\rm max}$. In the following, we therefore substitute $l_{\rm max}$ for l in the expression of the optical depth. We will discuss apart the particular case of rare close-by sources. One can evaluate the distance $l_{\rm max}$ in two ways: either as the energy loss distance $E|{\rm d}E/{\rm d}x|^{-1}$, or as the maximal distance that a particle can travel, assuming it has been detected with energy E and the maximal energy at the source is $E_{\rm max}$. In the following, we use this latter definition and assume $E_{\rm max} = 4 \times 10^{20}$ eV. The two definitions give values that never differ by more than 40% however, over the energy range 10^{17} eV $\rightarrow 10^{20}$ eV.

If particles diffuse rather than travel rectilinearly, the maximum distance is instead determined by $\sqrt{2Dt_{\rm max}}$, where D denotes the diffusion coefficient and $t_{\rm max} = l_{\rm max}/c$. This will be discussed in more detail in Sec. III C 2.

We may now plot the optical depths to scattering τ and $\tau_{\rm eff}$ as functions of energy. In Fig. 1, we show an example that ignores all scattering centers except magnetized galactic winds, for which we assume $n_{\rm gw} = 10^{-2}$ Mpc^{-3}, $r_{\rm gw} = 0.8$ Mpc, $B_{\rm gw} = 3 \cdot 10^{-8}$ G, and $\lambda_{\rm gw} = 0.05$ Mpc. The resulting optical depth τ is shown as the dashed (blue) line, and the effective optical depth $\tau_{\rm eff}$ as the solid (red) line. The dependence of τ on E actually reveals the dependence of $l_{\rm max}$ on E: $l_{\rm max}$ decreases sharply beyond a few 10^{19} eV as a consequence of pion production on the microwave background. The dependence of $\tau_{\rm eff}$ on E is even more pronounced, since the number of scatterings to achieve deflection of order unity rapidly increases with energy, roughly as E^2 beyond 10^{18} eV here [see Eq. (10)]. The horizontal dotted line indicates an optical depth of order unity, while the vertical dotted lines indicate at which energy $\tau_{\rm eff} = 1$ and $\tau = 1$ respectively, from left to right. As indicated on the figure, these lines delimit the energy ranges in which the Universe appears opaque, translucent of transparent to cosmic ray scattering. Interestingly, for this example, the Universe is translucent at energies close to the threshold for pion production $E_{\rm GZK} \simeq 6 \cdot 10^{19}$ eV [83,84].

In Fig. 2, we show the optical depths for the various types of scattering centers, taken in turn, and for two sets of parameters defining their characteristics, as indicated in the caption. In principle, one should of course sum the different optical depths of the types of scattering centers. If, however, the pollution of magnetized winds and radio halos permeate the filaments and nothing else, one should of course only consider the filaments as the sole scattering agents.

The two quantities $l_{\rm scatt}$ and $\bar{d}$ are shown together with the maximal path length (or source distance scale) $l_{\rm max}$ in Fig. 3 for magnetized galactic winds as scattering agents, with the same parameters used to construct Fig. 1. Figure 3 illustrates in a different way the opaque, translucent or transparent nature of the Universe to cosmic ray scattering.

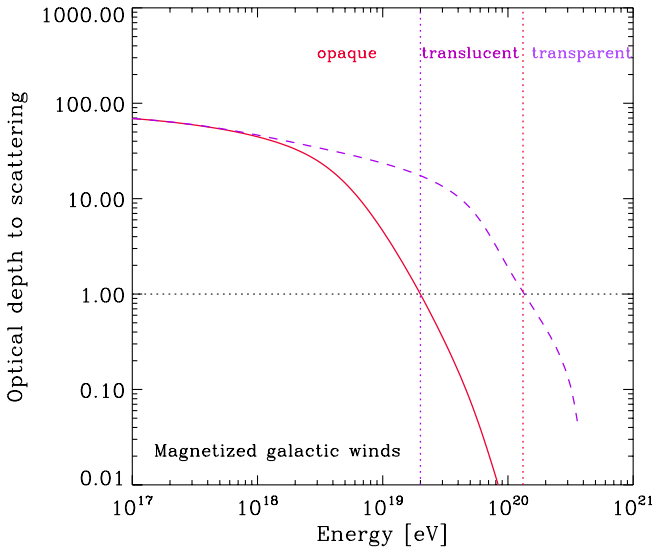

FIG. 1 (color online). Optical depth to cosmic ray scattering by magnetized galactic winds, with $n_{\rm gw} = 10^{-2}$ Mpc^{-3}, $B_{\rm gw} = 3 \cdot 10^{-8}$ G, $\lambda_{\rm gw} = 50$ kpc, and $r_{\rm gw} = 0.8$ Mpc. Solid line: optical depth $\tau_{\rm eff}$ to scattering by an angle of order unity, as defined in Eq. (10); dashed line: optical depth τ as defined in Eq. (6). In the energy range where $\tau > \tau_{\rm eff} > 1$, the Universe is opaque up to the energy loss distance; in the range where $\tau > 1 > \tau_{\rm eff}$, the Universe is translucent on this distance scale, meaning that cosmic rays suffer several to many scatterings, but the total angular deflection remains below unity; finally, at energies where $1 > \tau > \tau_{\rm eff}$, the Universe is transparent to cosmic ray scattering.

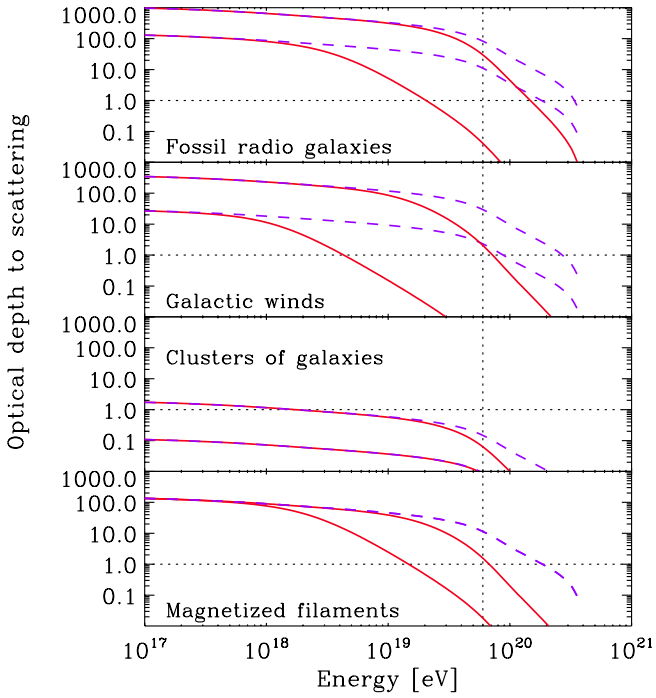

FIG. 2 (color online). Optical depth to cosmic ray scattering for different types of scattering agents and for two different sets of parameters in each case. Solid lines: optical depth $\tau_{\rm eff}$ to scattering by an angle of order unity, as defined in Eq. (10); dashed lines: optical depth τ as defined in Eq. (6). The vertical dotted line indicates $E = 6 \times 10^{19}$ eV. Fossil radio galaxies $n_{\rm rg} = 3 \cdot 10^{-3}$ Mpc^{-3}, $B_{\rm rg} = 10^{-8}$ G, $\lambda_{\rm rg} = 100$ kpc, and $r_{\rm rg} = 2$ Mpc (lower curves); $n_{\rm rg} = 10^{-2}$ Mpc^{-3}, $B_{\rm rg} = 10^{-7}$ G, $\lambda_{\rm rg} = 100$ kpc, and $r_{\rm rg} = 3$ Mpc (upper curves). Magnetized galactic winds $n_{\rm gw} = 10^{-2}$ Mpc^{-3}, $B_{\rm gw} = 10^{-8}$ G, $\lambda_{\rm gw} = 50$ kpc, and $r_{\rm gw} = 0.5$ Mpc (lower curves); $n_{\rm gw} = 5 \cdot 10^{-2}$ Mpc^{-3}, $B_{\rm gw} = 10^{-7}$ G, $\lambda_{\rm gw} = 50$ kpc, and $r_{\rm gw} = 0.8$ Mpc (upper curves). Clusters of galaxies $n_{\rm cg} = 10^{-5}$ Mpc^{-3}, $B_{\rm cg} = 10^{-6}$ G, $\lambda_{\rm cg} = 100$ kpc, and $r_{\rm cg} = 1$ Mpc (lower curves); $n_{\rm cg} = 10^{-5}$ Mpc^{-3}, $B_{\rm cg} = 10^{-7}$ G, $\lambda_{\rm cg} = 100$ kpc, and $r_{\rm cg} = 4$ Mpc (upper curves). Magnetized filaments of large scale structure: interseparation $d_{\rm f} = 25$ Mpc, $B_{\rm f} = 3 \cdot 10^{-9}$ G, $\lambda_{\rm f} = 300$ kpc, and $r_{\rm f} = 2$ Mpc (lower curves); $d_{\rm f} = 25$ Mpc, $B_{\rm f} = 3 \cdot 10^{-8}$ G, $\lambda_{\rm f} = 300$ kpc, and $r_{\rm f} = 2$ Mpc (upper curves).

One may also draw the analog of Fig. 2 for the distance to the last scattering surface $\bar{d}$ for the different types of scattering centers, as done in Fig. 4.

C. Inhomogeneity of the large scale structure—analytic discussion

The above results should be corrected for the presence of inhomogeneity when the distances considered are smaller than the inhomogeneity length 100 Mpc. In a first approach, one may assume that all scattering centers are clustered in the filaments of large scale structure. This affects transport in two ways: the typical distance to an interaction becomes of order $d_{\rm f}$ rather than d_i, but the typical deflection may be enhanced, as the probability of hitting more than one scattering center during the interaction with a filament is itself increased.

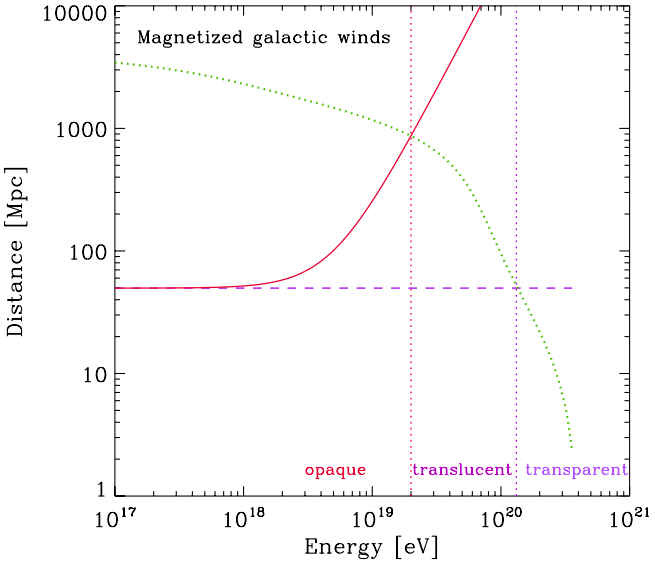

FIG. 3 (color online). Distance to the last scattering surface by magnetized galactic winds, with $n_{\rm gw} = 2 \cdot 10^{-2}$ Mpc^{-3}, $B_{\rm gw} = 3 \cdot 10^{-8}$ G, $\lambda_{\rm gw} = 50$ kpc, and $r_{\rm gw} = 0.8$ Mpc as in Fig. 1. Solid line: scattering length $l_{\rm scatt}$ for a deflection of order unity, as defined in Eq. (8); dashed line: distance $\bar{d}$ to the last scattering surface as defined in Eq. (5). The dotted (green) line indicates the maximal distance to the source $l_{\rm max}$, which also gives the source distance scale. In the energy range where $\bar{d} < l_{\rm scatt} < l_{\rm max}$, the Universe is opaque; in the range where $\bar{d} < l_{\rm max} < l_{\rm scatt}$, the Universe is translucent on the distance scale $l_{\rm max}$, meaning that cosmic rays suffer several to many scatterings, but the total angular deflection remains below unity; finally, at energies where $l_{\rm max} < \bar{d} < l_{\rm scatt}$, the Universe is transparent to cosmic ray scattering.

As the density of scattering centers in a filament becomes $n_{i|\rm f} = n_i/f_{\rm f}$, where $f_{\rm f} \sim 5\%$ is the average filament filling factor in the Universe, the mean free path to interaction inside a filament becomes $f_{\rm f} d_i$. Consequently, the average number of interactions $N_{\rm int|f}$ with scattering centers of type i during the ballistic crossing of a filament of radius $r_{\rm f}$ is

$$N_{\rm int|f} = \frac{\bar{r}_{\rm f}}{f_{\rm f} d_{\rm i}}, \tag{13}$$

where $\bar{r}_{\rm f}$ is the characteristic path length of the particle through the filament [see the discussion that follows Eq. (9) and the appendix]. This formula assumes that the particle suffers a deflection angle much smaller than unity at each interaction. The particle thus exits the filament with a total deflection and time delay (with respect to straight line crossing)

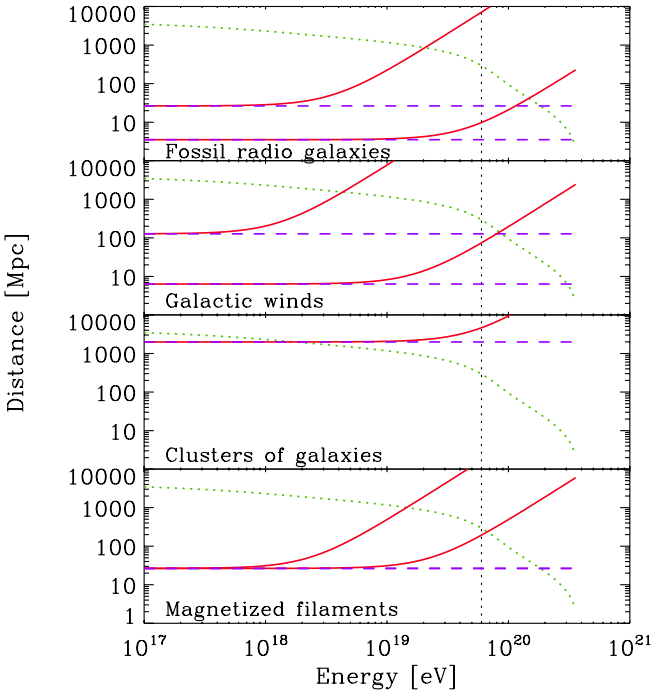

FIG. 4 (color online). Distance to the last scattering surface for different types of scattering agents and for two different sets of parameters in each case. Solid lines: scattering length $l_{\rm scatt}$ for deflection of order unity, as defined in Eq. (8); dashed lines: distance $\bar{d}$ to the last scattering surface as defined in Eq. (5). The dotted (green) line indicates the source distance scale $l_{\rm max}$. The vertical dotted line indicates the location of $E_{\rm GZK}$. Fossil radio galaxies: $n_{\rm rg} = 3 \cdot 10^{-3}$ Mpc^{-3}, $B_{\rm rg} = 10^{-8}$ G, $\lambda_{\rm rg} =$ 100 kpc, and $r_{\rm rg} = 2$ Mpc (lower curves); $n_{\rm rg} = 10^{-2}$ Mpc^{-3}, $B_{\rm rg} = 10^{-7}$ G, $\lambda_{\rm rg} = 100$ kpc, and $r_{\rm rg} =$ 3 Mpc (upper curves). Magnetized galactic winds: $n_{\rm gw} = 10^{-2}$ Mpc^{-3}, $B_{\rm gw} = 10^{-8}$ G, $\lambda_{\rm gw} = 50$ kpc, and $r_{\rm gw} =$ 0.5 Mpc (lower curves); $n_{\rm gw} = 5 \cdot 10^{-2}$ Mpc^{-3}, $B_{\rm gw} = 10^{-7}$ G, $\lambda_{\rm gw} = 50$ kpc, and $r_{\rm gw} = 0.8$ Mpc (upper curves). Clusters of galaxies: $n_{\rm cg} = 10^{-5}$ Mpc^{-3}, $B_{\rm cg} = 10^{-6}$ G, $\lambda_{\rm cg} = 100$ kpc, and $r_{\rm cg} = 1$ Mpc (lower curves); $n_{\rm cg} = 10^{-5}$ Mpc^{-3}, $B_{\rm cg} = 10^{-7}$ G, $\lambda_{\rm cg} = 100$ kpc, and $r_{\rm cg} =$ 4 Mpc (upper curves). Magnetized filaments of large scale structure: interseparation $d_{\rm f} = 25$ Mpc, $B_{\rm f} = 3 \cdot 10^{-9}$ G, $\lambda_{\rm f} = 300$ kpc, and $r_{\rm f} = 2$ Mpc (lower curves); $d_{\rm f} = 25$ Mpc, $B_{\rm f} = 3 \cdot 10^{-8}$ G, $\lambda_{\rm f} = 300$ kpc, and $r_{\rm f} = 2$ Mpc (upper curves).

$$\delta\theta^2_{i|\rm f} = N_{\rm int|f}\delta\theta^2_i, \tag{14}$$

$$\delta t_{i|\rm f} = N_{\rm int|f}\delta t_i + \delta\theta^2_{i|\rm f}\frac{\bar{r}_{\rm f}}{6c}. \tag{15}$$

In these equations, $\delta\theta_i$ and δt_i denote, respectively, the deflection angle and time delay consecutive to an interaction with scattering center of type i, as discussed in the appendix, while $\delta\theta_{i|\rm f}$ and $\delta t_{i|\rm f}$ give the corresponding deflection angle and time delay after the crossing of a filament.

In the opposite diffusive regime, in which $\delta\theta_i^2 \sim 1$, the particle follows a random walk. If the interaction length $f_{\rm f} d_i$ in the filament is much smaller than the filament radius $r_{\rm f}$, then the analysis of diffusive propagation in a filament conducted in Sec. A 2 applies. The particle bounces on the filament and exits on a timescale $r_{\rm f}/c$ at a distance $\sim(f_{\rm f} d_i/r_{\rm f})^{1/2} r_{\rm f}$ away from its point of first impact.

Note that the filling factor of the magnetized halos in the filament is $f_i/f_{\rm f}$, with $f_i \simeq (4/3) n_i \sigma_i r_i$ the average filling factor of scattering centers in the Universe. The filament becomes overfilled by the halos when $f_i \gtrsim f_{\rm f}$, or equivalently $N_{\rm int|f} \gtrsim (3\pi/16)^2 r_{\rm f}/r_{\rm i}$. If this condition is satisfied, one needs not consider the multiple interaction scenario depicted above, as it suffices to consider the filaments themselves as the scattering centers.

As mentioned above, the average distance to scattering is also modified if scattering centers cluster in filaments. It becomes $d_{i,\rm f}$

$$d_{i,\rm f} \simeq \frac{d_{\rm f}}{1 - \exp(-N_{\rm int|f})}, \tag{16}$$

as the denominator in this expression represents the probability of hitting a scattering center when the particle hits a filament. The quantities $d_{i,\rm f}$, $\delta\theta_{i|\rm f}$, and $\delta t_{i|\rm f}$ suffice in principle to characterize the transport of the particle in this structured Universe and to derive the phenomenological consequences with respect to experimental data. To gauge the influence of the geometry, one should compare the above quantities to those expected for a homogeneous scattering center distribution for typical values of the parameters. One finds

$$N_{\rm int|f} \simeq 1.3\left(\frac{\bar{r}_{\rm f}}{2\ {\rm Mpc}}\right)\left(\frac{f_{\rm f}}{0.05}\right)^{-1}\left(\frac{d_i}{32\ {\rm Mpc}}\right)^{-1}. \tag{17}$$

For the fiducial values used in Eq. (17), $f_i/f_{\rm f} = 0.83$, i.e. the halos barely overfill the filaments. This means that if r_i or n_i is larger than the quoted values, one must consider that the scattering centers are the filaments themselves, with the average quantities $d_{\rm f}$, $r_{\rm f}$, and $B_{\rm f}$ discussed previously. Conversely, if r_i or n_i is smaller, one must follow the above multiple interaction scheme.

Finally, one can verify that on distance scales $\gg d_{\rm f}$, the number of interactions (hence, the angular deflection and time delay) converge toward those obtained in the homogeneous case (at least for rectilinear propagation). In effect, the filling factor of filaments can be written in terms of $r_{\rm f}$ and $d_{\rm f}$ as $f_{\rm f} \simeq (\pi/2) r_{\rm f}/d_{\rm f}$; therefore, over a length scale d, the particle suffers $N_{\rm int|f} d/d_{\rm f} \simeq d/d_{\rm i}$ interactions. Qualitatively, the number of interactions per filament crossing compensates for the different distance between two zones of interaction (i.e. filaments). The effect of clustering of the scattering centers should thus be important on distance scales $\lesssim$ 100–200 Mpc, since the distance between two filaments is of order 30 Mpc; beyond that

distance, one can use the results derived in the homogeneous limit (Sec.).

One cannot exclude *a priori* that an even more realistic description of the hierarchical clustering of matter would produce a sophisticated law of probability for the interaction path length, leading to nonstandard effects such as anomalous diffusion. A more realistic description should also account for more complex distribution laws for the scattering center parameters. Monte Carlo simulations of particle propagation in a "realistic" scattering center distribution are best suited to address such issues and to provide quantitative estimates of the effect of inhomogeneity on the transport.

In the following section, we describe the simulations we have performed in order to study the influence of a realistic spatial distribution of scattering centers. In view of the uncertainties surrounding the origin of extragalactic magnetic fields and the parameters describing the scattering centers, we simply describe these latter with average values, as discussed in Sec. II.

D. Inhomogeneity of the large scale structure—numerical simulations

We have performed our simulations using a variant of the numerical code described in Ref. [46]. The simulation of the dark matter density field has been produced by the RAMSES code [85], and was kindly provided to us by S. Colombi; its characteristics are 256^3 cells, with extent 280 Mpc, giving a grid size 1.1 Mpc. For each simulation, we sample a population of scattering centers. We adopt two physically motivated bias models: in the first model, the scattering center density is proportional to the dark matter density field; in the second, the same proportionality applies, but we do not allow scattering centers to reside in regions with dark matter density $\rho < 0.5\langle\rho\rangle$. This latter model enhances the segregation of scattering centers in the large scale structure.

Figure 5 shows an example of a scattering center distribution in a two-dimensional slice of the simulation box in the first bias model. The segregation of scattering centers in filaments of the large scale structure is apparent, although some tend to reside in smaller density regions as a result of the large volume fraction occupied by such regions. Out of simplicity, each scattering center is modeled as a cube of the size of a cell of the simulation; each cell in the simulation is thus occupied by zero or one scattering center.

We then follow the trajectories of cosmic rays of various energies, using the method of Ref. [46], which simulates the transport of particles across cells of coherence of the magnetic field in both the diffusive and nondiffusive regime. These simulations allow to compute the various statistical properties of transport. A first effect brought to light by these simulations is the general increase in the length of first interaction in the inhomogeneous case, when compared with the homogeneous scattering center distribution. This increase is of order 40% for the first bias model, and about 60% for the second bias model. It does not seem to depend strongly on the scattering center density.

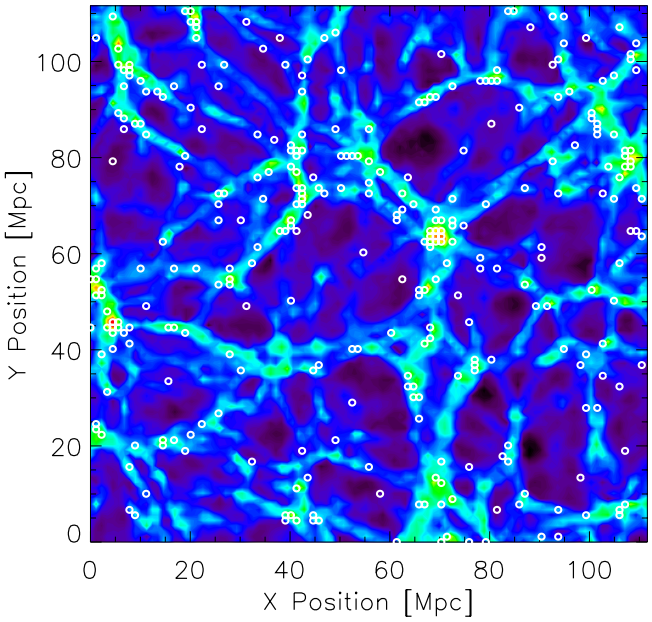

FIG. 5 (color online). Distribution of scattering centers in the large scale structure (in white), in a model in which the density of scattering centers follows that of dark matter (density contrast represented in colors). The thickness of this slice is 1.1 Mpc. The average density is 10^{-2} Mpc^{-3}.

Another significant effect is related to the source environment. If this latter is dense, as one might expect, the local scattering center density is higher than average, and therefore the cosmic ray may experience several interactions in the source environment in the first megaparsecs. Accordingly, the probability distribution for the first interaction departs from a simple exponential law: it exhibits a peak in the first Mpc, then decreases as an exponential. These extra interactions will not affect strongly the total deflection angle as seen from the detector, since 1 Mpc seen from 100 Mpc is subtended by an angle 0.6°. The time delay associated to this displacement is relatively small, being of order $\simeq r\delta^2/(2c) \simeq 180$ yr$(r/1$ Mpc$)(\delta/0.6°)^2$ (r denotes here the size of the structure in which the source is embedded, and δ the deflection angle associated to the displacement within this structure).

This effect is apparent in Fig. 6, which shows the average number of interactions as a function of distance, for different energies. The dashed lines indicate the corresponding trends for a homogeneous scattering distribution, which go to zero when the traveled distance tends to zero. On the contrary, the solid lines, which correspond to the simulated inhomogeneous case, depart from this scaling and indicate a fixed number of interactions, of order 2. The exact number turns out to depend on the environment

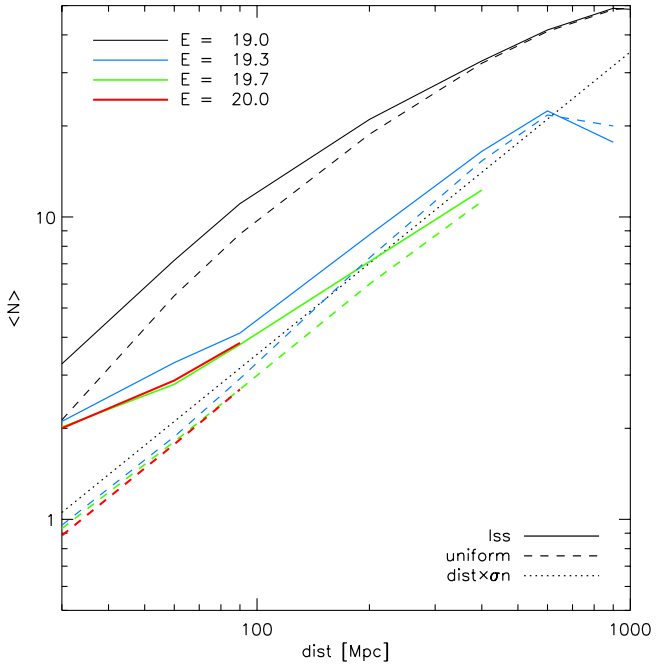

FIG. 6 (color online). Average number of interactions with scattering centers as a function of distance traveled in a time $t_{\max}(E)$. From top to bottom, solid lines correspond to different energies (in increasing order), as indicated in the colored version. Dashed lines indicate the numerical results for a homogeneous scattering center population, while solid lines correspond to the inhomogeneous case for which the scattering centers are distributed according to the dark matter density. The dotted line indicates the analytical homogeneous result for nondiffusive propagation. The scattering center density is such that $d_i = 32$ Mpc. Each scattering center is endowed with a magnetic field $B_i = 3 \cdot 10^{-8}$ G and coherence length $\lambda_i = 100$ kpc (due to the cubic geometry of the scattering center, this corresponds to $B_i = 2.7 \times 10^{-8}$ G and $\lambda_i = 100$ kpc in a spherical cell of radius 1 Mpc).

density and has a variance of order unity. For a source in an environment of average density, the number of such extra interactions in the source surroundings is negligible.

Figure 6 also reveals other interesting features. In particular, one can see clearly that the average number of interactions in the inhomogeneous case converges toward that obtained in the homogeneous case on distance scales $\gtrsim$ 100–200 Mpc, as expected [see the discussion that follows Eq. (17)]. For the highest energies, namely $E = 10^{19.7}$ eV and $E = 10^{20}$ eV, there is a slight offset between the analytical prediction for d_i and the homogeneous calculation; this difference is attributed to the cubic geometry of the scattering center. Particles of lower energies, in particular $E = 10^{19}$ eV, diffuse in the scattering center distribution, as evidenced by the higher slope of the average number of interactions as a function of the traveled distance l. One can check, in particular, that $N_{\rm int} \sim (l/d_i)^2$ as expected. At very large distances, this relation breaks down because the trajectory is cut after a time $t_{\max}$; hence, less and less particles are able to travel beyond a distance $\sim (ct_{\max})^{1/2} d_i^{1/2}$. Similar features are observed in the second bias model.

Finally, the same simulations can be used to compute the average deflection angle as a function of energy and traveled distance. This calculation is performed as follows. At a predetermined distance l, one draws at random a certain number of "small spheres" positioned on the sphere of radius l around the source. These small spheres mimic the detectors located at distance l from the source. There must be a sufficient number of these small spheres to guarantee a sufficient signal, but not so many that they would overlap, in which case one would oversample the sphere of radius l. Each time a trajectory intersects one of these spheres, the angle between the particle incoming direction in this sphere and the source location is recorded. Iterating over the particles and the small spheres allows to reconstruct the probability distribution of deflection angles.

The result is shown in Fig. 7 for various energies, for the same inhomogeneous distribution of scattering centers as above. Each cell is endowed with a magnetic field of strength $B_i = 3 \times 10^{-8}$ G and of coherence length $\lambda_i = 100$ kpc. Since the cell is cubic, of size 1.1 Mpc, the

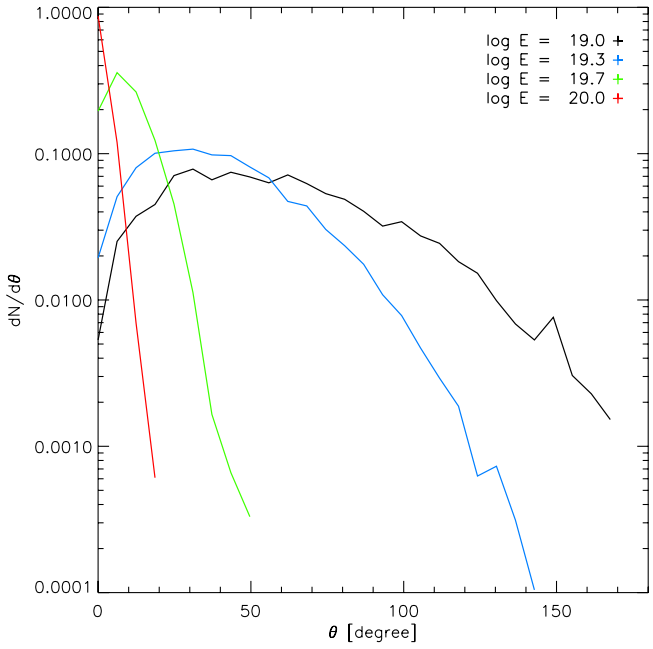

FIG. 7 (color online). Histogram of deflection for different energies, as indicated. The values have been computed at different distances for the different energies: 1000 Mpc for $E = 10^{19}$ eV, 600 Mpc for $E = 10^{19.3}$ eV, 400 Mpc for $E = 10^{19.7}$ eV, and 90 Mpc for $E = 10^{20}$ eV. As before, the scattering center density is such that $d_i = 32$ Mpc. Each scattering center is endowed with a magnetic field $B_i = 3 \cdot 10^{-8}$ G and coherence length $\lambda_i = 100$ kpc (due to the cubic geometry of the scattering center, this corresponds to $B_i = 2.7 \times 10^{-8}$ G and $\lambda_i = 100$ kpc in a spherical cell of radius 1 Mpc).

deflection per interaction corresponds to that obtained for a spherical cell of radius 1 Mpc and magnetic field strength $B_i = 2.7 \times 10^{-8}$ G. The values shown in Fig. 7 have been computed at the following distances: 1000 Mpc for $E = 10^{19}$ eV, 600 Mpc for $E = 10^{19.3}$ eV, 400 Mpc for $E = 10^{19.7}$ eV, and 90 Mpc for $E = 10^{20}$ eV. These distances are representative of $l_{\rm max}$, hence, of the source distance scale. At an energy $E = 10^{20}$ eV, the mean and median deflections are of order 3° and 2.6°, respectively, while at $E = 10^{19.7}$ eV, they increase to 12° and 11.5°, and become larger at smaller energies. These values are about 30% smaller than those expected from the analytical calculation, given in Eq. (21) further below. This difference can stem from the slightly different number of interactions experienced by particles in the inhomogeneous scattering center distribution, as compared with the homogeneous case (see Fig. 7). The cubic geometry of scattering centers used in our simulation can also contribute to alter the values of the deflection angles. Obviously, these deflections could also be larger or smaller depending on the exact values of the scattering center characteristics (see discussion above).

To summarize this discussion on the effect of inhomogeneity, we note the following features: when the scattering centers correlate with the large scale structure, the probability law of first interaction and the number of interactions departs from those obtained in the homogeneous case, at distances $\lesssim 100$ Mpc. The difference between the two cases depends on several factors: the source environment and the bias of the scattering center distribution with respect to the underlying dark matter distribution, in particular. It is found, however, that on large scales $\gtrsim$ 100 Mpc and in the weak deflection regime, one recovers the results of the homogeneous scattering center distribution discussed in Sec. .

Extra interactions in the source environment, if sufficiently dense to be populated by scattering centers, may increase slightly the time delay with respect to straight line propagation but will not modify substantially the total deflection angle. In the diffusive regime, scattering occurs against filaments if the interaction length in the filament is smaller than the filament size, or against the scattering centers, if not.

III. CONSEQUENCES FOR COSMIC RAY TRANSPORT

In this section, we discuss the phenomenological consequences of the above model of cosmic ray transport with respect to the signatures of different source models, discussing, in particular, the absence or existence of counterparts. We will discuss in Sec. IV the interpretation of existing data in the light of these consequences, and, in particular, the recent correlation announced by the Pierre Auger Observatory.

A. Optically thin regime

The optically thin regime, in which $l_{\rm max} < \bar{d} < l_{\rm scatt}$, is trivial in terms of particle propagation: most particles travel in a straight line, without interacting in the intergalactic medium; therefore, one should expect to see the source directly in the arrival direction of the highest energy events. However, in the case of gamma-ray burst sources, the spreading of arrival times through the interaction with cosmic magnetic fields is essential to reconcile the gamma-ray burst rate with the rate of ultrahigh energy cosmic ray detection [86]. In the absence of scattering (hence, time delay), such a bursting source would be essentially unobservable as the occurrence rate is much too low when compared with the lifetime of the experiment.

Independently of the source scenario, there does not exist at present clear and unique evidence for counterpart identification, as discussed briefly in the introduction. Extra deflection could arise from an all-pervading intergalactic magnetic field or the galactic magnetic field. The influence of an all-pervading intergalactic magnetic field has been discussed in previous works, see for instance Refs. [40,41,45,51] for recent works. Note that our model of magnetized filaments and nonmagnetized voids may be considered as an approximation to the more realistic magnetic field configurations derived in these studies.

Concerning the influence of the galactic magnetic field, existing models suggest that the typical deflection at the highest energies, say $\simeq 10^{20}$ eV, are probably of the order of a few degrees [87,88]. Hence, one would need to invoke the existence of an extended magnetized halo to provide sufficient deflection. Alternatively, one may consider a scenario in which most particles at the highest energies are heavy nuclei, which are more easily deflected.

B. Translucent regime

The intermediate regime, in which $\bar{d} < l_{\rm max} < l_{\rm scatt}$ is interesting, because the typical deflection is smaller than unity, yet it could be sufficient to explain the lack of counterpart.

1. Transport

Since the total deflection remains smaller than unity, one may describe the transport as near-ballistic with a nonzero time delay as measured relatively to straight line propagation. Furthermore, one may use in this case the time delay and deflection formulae obtained from random walk arguments in Ref. [14], provided one accounts for the inhomogeneity of the magnetic field. In detail, at each scattering with scattering center i, the particle suffers and angular deflection $\delta\theta_i$ and exits with a delay δt_i. The corresponding formulae for $\delta\theta_i$ and δt_i are given in Eqs. (A4) and (A6).

The total time delay δt acquired over a path length l is given by the sum of the time delays acquired during each

scattering as well as that resulting from the fact that the particle does not travel in a straight line from the source to the detector. If the particle is seen from the detector at a typical deflection angle $\delta\alpha$ away from the source direction, then the time delay associated to this transverse displacement with respect to the line of sight is $l\delta\alpha^2/(4c)$ [89]. In the limit of large optical depth $\tau > 1$, this angle $\delta\alpha^2$ is written as [89]

$$\delta\alpha^2 = \frac{\tau}{3}\delta\theta_i^2, \tag{18}$$

where $\delta\theta_i^2$ is the rms scattering angle per scattering event.

On average, the particle interacts at every step of length $\bar{d}$, with probability $\bar{d}/d_i$ of hitting a structure of type i. Then the total time delay and deflection acquired after traveling a path length l are

$$\delta\alpha^2 = \frac{\tau}{3}\sum_i \frac{\bar{d}}{d_i}\delta\theta_i^2, \tag{19}$$

$$\delta t \simeq \tau\sum_i \frac{\bar{d}}{d_i}\delta t_i + \frac{l\delta\alpha^2}{4c}. \tag{20}$$

To make simple estimates, consider the case in which one type of scattering event dominates the scattering history. Then, the typical deflection angle reads (still assuming $\tau > 1$)

$$\delta\alpha \simeq 1.7^\circ\left(\frac{\tau}{3}\right)^{1/2}\left(\frac{\bar{r}_i}{2\ \mathrm{Mpc}}\right)^{1/2}\left(\frac{B_i}{10^{-8}\ \mathrm{G}}\right)\left(\frac{\lambda_i}{0.1\ \mathrm{Mpc}}\right)^{1/2} \times\left(\frac{E}{10^{20}\ \mathrm{eV}}\right)^{-1}, \tag{21}$$

where $\bar{r}_i$ is the characteristic size of the scattering center [see after Eq. (9) and the appendix]. The optical depth to cosmic ray scattering is related to the distance and the geometrical characteristics of the scattering centers as in Eq. (7). This deflection may thus be non-negligible for typical parameters of the scattering centers discussed in the previous section. In all cases, the arrival direction should point back to the last scattering center encountered by the cosmic ray. Since scattering centers are highly magnetized regions, and as such are probably associated with active objects such as radio galaxies, one may be deceived by their presence on the line of sight, and interpret them as the source of ultrahigh energy cosmic rays. The smoking gun of such counterfeiting is the distance scale to these objects: in this optically thick regime, most counterparts would be located at a distance scale $\bar{d}$ (which can be measured) significantly smaller than the expected distance scale l_{max} (which is known).

The associated time delay reads

$$\delta t \simeq 7.0\times 10^4\ \mathrm{yrs}\left(\frac{l}{100\ \mathrm{Mpc}}\right)\left(\frac{\delta\alpha}{1.7^\circ}\right)^2. \tag{22}$$

The second term on the right-hand side of Eq. (20) indeed dominates largely over the first. It is easy to verify that the relation between $\delta\alpha^2$ (the rms angle between the line of sight to the source and the particle incoming velocity on the detector) and $\delta\theta^2$ (the rms velocity deflection angle per scattering) remains uncchanged in the limit $\tau < 1$. Obviously, however, the solid angle of the source images cannot exceed that of the scattering center.

Further effects related to the formation of angular images are discussed in the following.

2. Angular images

The physics of the formation of angular images has been discussed in detail in Refs. [14,16] in the case of ultrahigh energy cosmic rays propagating in an all-pervading irregular magnetic field. In the model under consideration, differences may occur when the discreteness of scattering centers cannot be neglected. This occurs if $\tau \lesssim 1$, since τ indicates the covering factor of the scattering centers.

In the limit $\tau \gg 1$, one may use the analysis of Refs. [14,16] provided one translates the quantities defined in these studies in terms of those relevant in the present case, such as the scattering rate per interaction determined in the appendix. One point of interest concerns the shape of the angular image. As discussed in Refs. [14,16], the image will be centered on the source, and broadened by an angle $\delta\alpha$, if there are many uncorrelated paths through the scattering medium linking the source to the detector. In the present case, this condition remains unchanged in the limit $\tau \gg 1$, i.e. it reads $l\delta\alpha \gg \lambda_i$, with λ_i the magnetic field coherence length of the scattering center. If $l\delta\alpha \ll \lambda_i$, the image will appear displaced from the true source position by an angle $\delta\alpha$, with a small dispersion. As discussed in Ref. [16], the distortion of the image does not modify (on average) the flux received from the source, in either limit considered above. This implies, in particular, that the presence of scattering centers does not modify the expected number of events, but only modifies the angular disposition of these multiple events.

The intermediate regime $l\delta\alpha \simeq \lambda_i$ is that multiple images and magnetic lensing amplification effects may become prominent (see Ref. [90] for a numerical demonstration of magnetic lensing). However, as λ_i is unlikely to exceed a few hundreds of kpc, this intermediate regime is to be expected only in the limit of very small deflection

$$\frac{l\delta\alpha}{\lambda_i} \simeq 29\left(\frac{l}{100\ \mathrm{Mpc}}\right)\left(\frac{\delta\alpha}{1.7^\circ}\right)\left(\frac{\lambda_i}{100\ \mathrm{kpc}}\right)^{-1}. \tag{23}$$

This equation indeed suggests that typical angular images should be broadened by $\delta\alpha$ and centered on the source location.

In the limit of small optical depth ($\tau \sim 1$), which becomes all the more relevant at the highest energies $E \sim 10^{20}$ eV, some noticeable differences can be expected. Two questions of interest are the shape of angular images,

and the possible magnification or demagnification of images. As we argue, these effects depend on the hierarchy between the typical displacement $\simeq l\delta\alpha$ in the scattering center plane (oriented perpendicular to the line of sight to the source), the size of the scattering center r_i, as well as the typical distance between two scattering centers in this plane, which is given by $(n_i l)^{-1/2}$. Out of simplicity, we assume spherical scattering centers; we will argue that the conclusions remain unchanged for filaments.

In order to study the limit $\tau \lesssim 1$, it suffices to assume that there is only one scattering center on the line of sight to the source. We further assume that this scattering structure is centered on the line of sight. The shape of the angular image is here as well determined by the ratio $l\delta\alpha_i/\lambda_i$. As we now argue, the flux received does not deviate from that expected in the absence of scattering, $F_0 = \dot{N}_{\rm UHECR}/(4\pi l^2)$, provided the scattering center is larger than the image of the source, i.e. $\delta\beta_i > \delta\alpha_i$, denoting by $\delta\beta_i \equiv r_i/l_1$ the typical apparent half-opening angle of the scattering center with l_1 the distance between the scattering center and the detector. If the opposite inequality holds ($\delta\beta_i < \delta\alpha_i$), the flux from the source gets demagnified through scattering. This can be seen as follows.

Each area element on the scattering structure can be assumed to dilute an incoming unidirectional flux into a beam of solid angle $\delta\Omega \simeq \pi\delta\theta_i^2$ (assuming small deflection). As seen from the source, this defines a solid angle $\delta\Omega_{|\rm s}$ such that, if particles are emitted within $\delta\Omega_{|\rm s}$, they may be redirected toward the detector through scattering. Then

$$\delta\Omega_{|\rm s} = \left(\frac{l_1}{l}\right)^2 \delta\Omega. \tag{24}$$

The ratio l_1/l corresponds to the ratio between the half-opening angle of the cone of solid angle $\delta\Omega_{|\rm s}$ to $\delta\theta_i$. Effects related to the finite size of the scattering center are considered further below.

Now, of the flux impinging on the area element, only a fraction $\delta\Omega_{\rm d}/\delta\Omega$ is diverted away toward the detector of solid angle $\delta\Omega_{\rm d} = A_{\rm d}/l_1^2$ and area $A_{\rm d}$ (this solid angle is measured relative to the scattering structure). One then finds that the flux received from the source is

$$\begin{aligned} F &= \frac{\dot{N}_{\rm UHECR}}{4\pi A_{\rm d}} \frac{\delta\Omega_{\rm d}}{\delta\Omega} \min\left(\delta\Omega_{|\rm s}, \frac{\pi r_i^2}{l_2^2}\right) \\ &= F_0 \min\left[1, \left(\frac{l}{l_1}\right)^2 \frac{r_i^2}{l_2^2 \delta\theta_i^2}\right]. \end{aligned} \tag{25}$$

In this equation, $l_2 \equiv l - l_1$ represents the distance between the source and the scattering center. The "min" function has been introduced in order to limit the angular size of the source image to the minimum of the size produced by deflection and the size of the scattering center (which is seen through a solid angle $\pi r_i^2/l_2^2$ from the source).

Thus, $F = F_0$ if the solid angle $\delta\Omega_{|\rm s}$ is smaller than the solid angle of the scattering structure as seen from the source, which amounts to $\delta\alpha_i < \delta\beta_i$. This can be traced back to the compensation between a larger source image (which would lead to amplification) with the dilution of the signal into a beam of solid angle $\delta\Omega$.

If, on the contrary $\delta\alpha_i > \delta\beta_i$, the source image is demagnified by the ratio $F/F_0 \simeq \delta\beta_i^2/\delta\alpha_i^2$, i.e. by the ratio of the solid angle of the scattering center to the solid angle that the source image would have if the scattering center had an infinite extent. One can generalize this result to the case of filamentary scattering centers, by noting that the flux gets demagnified by the ratio of the area of the scattering center to the projected area (on the scattering plane) of the beam of solid angle $\delta\Omega_{|\rm s}$. Using previous fiducial values for the scattering centers, and assuming $l_2 = l/2$, one finds

$$\frac{\delta\alpha_i}{\delta\beta_i} \simeq 0.8\left(\frac{\delta\alpha_i}{1^\circ}\right)\left(\frac{l}{100\ {\rm Mpc}}\right)\left(\frac{r_i}{1\ {\rm Mpc}}\right)^{-1}. \tag{26}$$

However, this result considers only the influence of one scattering center on the line of sight. As the beam width exceeds the apparent size of the scattering center on the line of sight, one must take into account the possibility that a fraction of the beam interacts with scattering centers away from the line of sight. In the limit of small angle deflection, and still assuming $\delta\alpha_i > \delta\beta_i$, the flux received by the detector should be given by Eq. (25) above, multiplied by the number of scattering centers of the scattering plane intercepted by the beam of solid angle $\delta\Omega_{|\rm s}$. We neglect the possible overlap of the projected areas of the scattering centers, which corresponds to $(n_i l)^{-1/2} > r_i$, or equivalently $\tau < 1$. This number of intercepted scattering structures can then be written as

$$\begin{aligned} N_i &\simeq n_i l l_2^2 \delta\Omega_{|\rm s} \\ &\approx 0.96\left(\frac{n_i}{10^{-2}\ {\rm Mpc}^{-3}}\right)\left(\frac{l}{100\ {\rm Mpc}}\right)^3\left(\frac{\delta\alpha_i}{1^\circ}\right)^2. \end{aligned} \tag{27}$$

Hence, the flux received from all intercepted scattering centers in the limit $\delta\alpha_i > \delta\beta_i$ is

$$F_{\rm tot} \simeq N_i F \simeq \tau F_0. \tag{28}$$

This result can be understood as follows: the number of intercepted scattering centers is the product of the surface density $n_i l$ times the projected area (on the scattering plane) of the beam of solid angle $\delta\Omega_{|\rm s}$; however, the demagnification factor is the ratio of the scattering center area to this latter, so that the total demagnification factor is the product of the surface density of scattering centers times the area of one scattering center, i.e. τ. This argument remains unchanged for filamentary scattering centers.

Equation (28) gives the total demagnification of the flux from a source with one scattering structure on the line of sight, in the limits $\delta\alpha_i > \delta\beta_i$ and $(n_i l)^{-1/2} > r_i$ (i.e. $\tau < 1$). Interestingly, the angular image is now decomposed

into N_i distinct images of angular size $\delta\beta_i$ each, of similar flux $\sim F_0\tau/N_i$, being separated from one another by an angle of order $\delta\alpha_i$.

Note that, on average, there is neither magnification nor demagnification of the flux, as expected. Regarding the limit $\tau \gg 1$, this effect has been discussed in Ref. [16], in particular. Concerning the limit $\tau < 1$ discussed above, there are two possibilities. If $\delta\alpha_i < \delta\beta_i$, then as shown in Eq. (25) the flux is unchanged through scattering. If $\delta\alpha_i > \delta\beta_i$, the flux of the source is demagnified by τ through scattering, but this occurs with probability $\simeq \tau$, which corresponds to the possibility of having one scattering structure on the line of sight. There is also a probability $1 - \tau$ of seeing the source directly (without scattering) together with echoes of flux τF_0 associated to scattering with structures off the line of sight. Hence, the total flux is on average unchanged. Deviations from this average may occur in certain configurations, for instance, through magnetic lensing, see Eq. (23) above and Ref. [16], or, in particular, source scenarios, as discussed at the end of Sec. III B 5 further below.

3. Experimental signatures for continuously emitting sources

As far as continuously emitting sources are concerned, a possibly large angular deflection could prevent the detection of counterparts. Indeed, values such as $d_i = 30$ Mpc and $B_i = 10^{-8}$ G suffice to produce a deflection of order 10° over a path length $l = l_{\rm max}$ at energy $4 \cdot 10^{19}$ eV, which is a generic threshold energy used in the search for counterparts. The strong evolution of $\delta\theta$ with energy results from the strong evolution of $l_{\rm max}$ with E close to the threshold for pion production. This suggests that counterparts should be found at sufficiently high energies, which of course asks for high statistics.

Since the flux received from sources within distance l scales as l, one may expect to see the source in the arrival directions of a subset $l_0/l_{\rm max}$ of all events, l_0 being defined as the distance at which the typical deflection becomes comparable to the radius within which one searches for counterparts. This number $l_0/l_{\rm max}$ should be smaller than unity, since if it were unity, it would mean that the total angular deflection for all sources is very small, hence, that counterparts should have been detected.

4. Experimental signatures for bursting sources

Regarding bursting sources, and gamma-ray bursts, in particular, Eq. (22) shows that the typical time delay is sufficiently large to explain the lack of temporal association between cosmic ray arrival directions and gamma-ray bursts, as well as the continuous rate of detection of high energy cosmic rays. Recall indeed that one potential difficulty of the gamma-ray burst scenario is to explain the near continuous detection of cosmic rays at the highest energies $\sim 10^{20}$ eV, when the gamma-ray burst rate is only $\sim 10^{-3}$ yr^{-1} within the energy loss distance ~ 100 Mpc. As noted by Waxman [86], this difficulty may be overcome if the arrival time spread σ_t of the highest energy events is sufficiently large, i.e. $\sigma_t \gtrsim 10^3$ yr at 10^{20} eV, in particular.

Following Ref. [14], we note that the magnitude of $\sigma_t/\delta t$ is influenced by the number of different trajectories that the particle can follow from the source to the detector. If indeed all particles follow the very same trajectory, $\sigma_t \ll \delta t$, while if different particles may follow different trajectories, one should expect $\sigma_t \sim \delta t$. In the present model, Eq. (23) shows that the latter situation is much more likely, so that $\sigma_t/\delta t \sim 1$. Furthermore, broadening of the time signal at the highest energies is likely to be increased by stochastic pion production, which results in $\sigma_t/\delta t \sim 1$ [23].

One may also calculate the number of gamma-ray burst sources, which can contribute to the flux at a given energy E [14,91]

$$N_{\rm GRB}(E) \simeq \dot{n}_{\rm GRB}\,\frac{2\pi}{5}\,l_{\rm max}^3\,\sigma_t. \tag{29}$$

This number of apparent gamma-ray bursts in the cosmic ray sky characterizes the amount of statistical fluctuation to expect around the mean flux at a given energy [14]. Using Eq. (22), one obtains

$$N_{\rm GRB}(E) \simeq 88\left(\frac{\tau}{3}\right)\left(\frac{l_{\rm max}}{100\ {\rm Mpc}}\right)^4\left(\frac{\bar{r}_i}{2\ {\rm Mpc}}\right)\left(\frac{E}{10^{20}\ {\rm eV}}\right)^{-2} \times \left(\frac{B_i}{10^{-8}\ {\rm G}}\right)^2\left(\frac{\lambda_i}{0.1\ {\rm Mpc}}\right)\left(\frac{\dot{n}_{\rm GRB}}{10^{-9}\ {\rm Mpc}^{-3}\cdot{\rm yr}^{-1}}\right) \times \frac{\sigma_t}{\delta t}. \tag{30}$$

The magnitude of this number of apparent sources implies that the spectrum of ultrahigh energy cosmic rays should not reveal statistical fluctuations until energies as large as a few 10^{20} eV, at least for these fiducial values that characterize the scattering centers.

5. Direction dependent effects

Since the sources of protons with energies beyond the pion production threshold are bound to reside within 100–200 Mpc, one may expect the optical depth of scattering centers to vary with the direction of observation, just as the density of matter. In order to discuss the influence of such variation on existing and upcoming data, we have constructed sky maps of the matter concentration using the Point Source Catalogue of galaxies [92], which presently offers the most adequate survey for this task.

The integrated column density of baryonic matter up to a distance l is shown in Fig. 8 for different maximal distances: $l = 40$, 80, 120, 160 Mpc (we adopt $H_0 = 70$ km/s/Mpc). In order to correct for the incompleteness of the catalog, we have followed the prescriptions of Ref. [92] and smoothed the galaxy distribution with a variable Gaussian filter, making use of the HEALPix li-

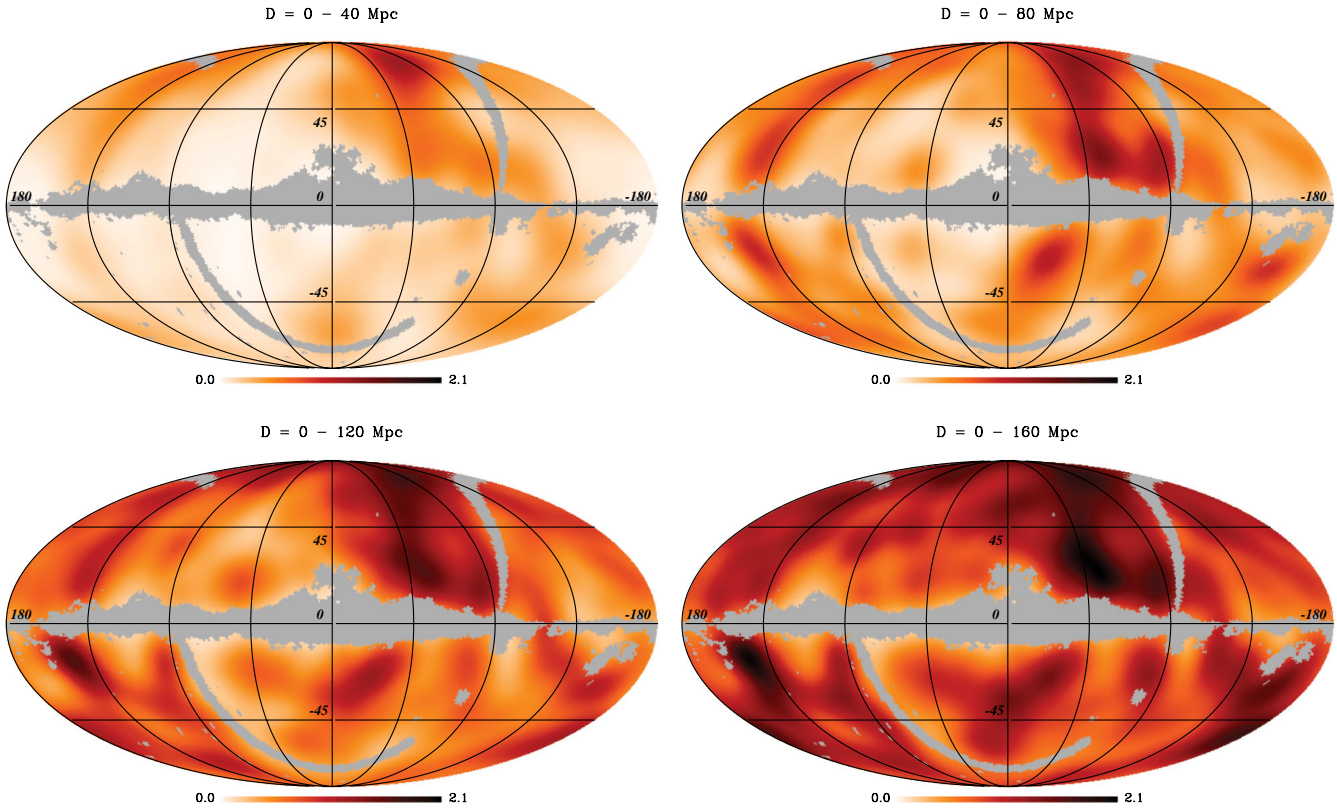

FIG. 8 (color online). Integrated galaxy column density as derived from the PSCz catalog of galaxies up to the maximal distances $l = 40$ Mpc, $l = 80$ Mpc, $l = 120$ Mpc, and $l = 160$ Mpc from left to right and top to bottom (Mollweide projection). The contours give the column density N_g in units of the mean column density $\langle N_g \rangle = \langle n_g \rangle \times 160$ Mpc, with $\langle n_g \rangle$ the mean galaxy density. The gray mask indicates the regions of the sky that are not covered by the PSCz catalog [92].

brary [93]. The overall resolution of the maps is of order 7°.

These maps provide an estimate of the optical depth to cosmic ray scattering in the case in which the scattering centers are distributed as the galaxies. If their distribution is biased with respect to that of n_g, for instance, $n_i/\langle n_i \rangle = b_i(n_g/\langle n_g \rangle)$, then the optical depth is expressed as the following function of $N_g/\langle N_g \rangle$:

$$\tau = \langle n_i \rangle \sigma_i l \frac{\int \mathrm{d}l b_i(n_g/\langle n_g \rangle)}{\int \mathrm{d}l n_g/\langle n_g \rangle} \frac{N_g}{\langle N_g \rangle}, \tag{31}$$

and the prefactor $\langle n_i \rangle \sigma_i l = \langle \tau \rangle$, see also Eq. (7). The quantity $N_g/\langle N_g \rangle$ is that plotted in Fig. 8 for a distance $l = 160$ Mpc. This figure assumes no bias, in which case $\tau = \langle \tau \rangle N_g/\langle N_g \rangle$. Therefore, in order to read off τ from Fig. 8 and the above formula, one should use $l = 160$ Mpc in the definition of $\langle \tau \rangle$ together with the inferred value of $N_g/\langle N_g \rangle$ from Fig. 8. If the bias were not trivial, meaning $b_i(n_g/\langle n_g \rangle) \neq 1$, its main effect would be to increase the contrast of Fig. 8. Figures for particular situations can be provided upon demand.

The above fiducial values for the scattering centers reveal an important point: depending on the direction of observation, one may be in a regime of small optical depth $\tau < 1$ or large optical depth $\tau > 1$. This has several noteworthy consequences.

First of all, the typical deflection angle becomes itself direction dependent. In particular, the values used in Eq. (21) correspond to $\langle \tau \rangle = 3$ and $\delta\alpha \propto \tau^{1/2}$. This simple scaling law along with Fig. 8 allow to estimate, as a function of the parameters characterizing the scattering centers, the typical deflection angle in different parts of the sky.

A sky map of deflection angles had been provided previously in Ref. [39], using a constrained numerical simulation of the local Universe with an all-pervading (albeit inhomogeneous) magnetic field whose initial data was fixed at high redshift. One advantage of the present maps shown in Fig. 8 is to parametrize the expected deflection in terms of the properties of the scattering structures; in this sense, the above maps are more general. Ref. [44] has also provided a similar map, using the PSCz galaxy catalog to construct the matter density field, and scaling the magnetic field to the matter density through the law $B \propto \rho^{2/3}$. The exponent 2/3 assumes isotropic compression of the magnetic field during structure formation, and it seems that numerical simulations indicate a more sophisticated law, with an exponent closer to 1 (see discussion in Refs. [46,52]). Ref. [44] also reconstructs the

galaxy density field on small scales by repopulating randomly the galaxy distribution using the density distribution from the PSCz on larger scales, so that their map is influenced by this reconstruction on scales smaller than $\sim 7^\circ$.

Following the discussion of Sec. III B 2, the flux of a source does not get demagnified nor magnified, up to possible magnetic lensing effects, as it crosses a region of scattering centers, provided the predicted apparent size of the source image does not exceed that of the scattering structure. It will, however, suffer demagnification in the opposite limit. Note that this does not contradict the fact that an isotropic distribution of sources will yield isotropic arrival directions on the detector provided that all arrival directions from the detector can be backtracked to infinity. Indeed, if a particular region of the sky is associated with a particularly large angular deflection, the flux of any point source is diluted by deflection through the crossing of this structure; however, this deflection also opens a larger solid angle on the source plane, so that a larger number of sources can contribute, and both effects compensate each other. This fact has been discussed, in particular, in Ref. [94] with respect to ultrahigh energy cosmic ray propagation in the galactic magnetic field.

As mentioned in Ref. [94], one loop hole of the above argument is the possible existence of so-called bottle orbits, which do not connect the detector to infinity. However, one does not expect this effect to appear at the ultrahigh energies under consideration in view of the (nearly) random and sporadic distribution of the scattering centers throughout the Universe and in view of the random nature of the deflection suffered at each interaction. This assertion could be verified using dedicated numerical simulations of particle propagation.

Just as angular deflection, the time delay will depend on direction, as $\delta t \propto \tau$. Although the magnitude of the time delay (more precisely, of its variance) controls the number of bursting sources that can be seen at a given time, it does not influence the flux received as long as $N_{\rm GRB} \gg 1$. Indeed, a larger δt means a larger $N_{\rm GRB}$ (at a fixed value of $\sigma_t/\delta t$), but the flux of each gamma-ray burst is decreased accordingly by the larger σ_t and both effects compensate each other exactly. However, if at a given energy $N_{\rm GRB} \lesssim 1$ in a certain region of the sky, one should observe a corresponding cutoff in the energy spectrum from this region of the sky, hence, a reduced number of events.

As a clear example of the above possibility, consider a region of the sky, of solid angle $\Delta\Omega$, in which the average optical depth to cosmic ray scattering $\tau < 1$. Then any source has a probability $\simeq \tau$ of having one scattering center on the line of sight, and therefore being seen if the time delay is sufficient. If there is no scattering center on the line of sight (with probability $1 - \tau$), then the time delay is zero (in a first approximation), so that the probability of observing a source within $\Delta\Omega$ and up to a distance l within the lifetime of an experiment $\Delta t_{\rm exp} \sim 10$ yrs is extremely small

$$P = \frac{1}{3}\Delta\Omega l^3 \dot{n}_{\rm GRB}\Delta \simeq 3\times 10^{-4}\frac{\Delta\Omega}{0.1\ {\rm str}}\frac{\dot{n}_{\rm GRB}}{10^{-9}\ {\rm Mpc}^{-3}\,{\rm yr}^{-1}}\frac{\Delta t_{\rm exp}}{10\ {\rm yrs}}. \quad (32)$$

Note that 0.1 str corresponds to a region of half-opening angle $\simeq 10^\circ$. In practice, no source should be seen in this particular direction unless it resides in a highly magnetized environment [see discussion after Sec. II D, see also Eq. (A6)]. As argued in Sec. III B 2, one might see "echoes" of this source from scattering centers located away from the line of sight, provided $l\delta\alpha_i \gtrsim (n_i l)^{-1/2}$. Even then, however, the total flux of these secondary images would be demagnified by τ as compared with that expected from the source without scattering.

In summary, the average flux expected in this solid angle $\Delta\Omega$ is lower by a factor τ than that expected from regions in which the optical depth is greater than unity.

Conversely, if the source is not of the bursting type, one might see it directly in the arrival direction if this source lies in a hole of the foreground scattering center distribution.

C. Opaque regime

The opaque regime corresponds to $\tau > \tau_{\rm eff} > 1$. In this case, cosmic rays diffuse from the source to the detector as in a random billiard.

The energy spectrum received from a given source is likely to be strongly modified by the presence of strongly magnetized scattering centers, as discussed in Ref. [35]. Roughly, one should observe a low-energy cutoff at an energy $E_{\rm c}$ such that $\delta\theta_i^2 < 1$ for $E > E_{\rm c}$ and $\delta\theta_i^2 \sim 1$ at lower energies. However, when one considers the energy spectrum received from an ensemble of sources, whose flux interacts with an ensemble of scattering centers, one should calculate the diffuse average flux in order to make contact with the measured spectrum. This average spectrum should not differ from the spectrum corresponding to rectilinear propagation if the diffusion theorem applies [95] and magnetic horizon effects are unimportant, i.e. if the distance between two sources $n_{\rm s}^{-1/3}$ is smaller than the energy loss distance and the diffusion length. Otherwise, one should calculate the spectrum following the methods of Ref. [96] with the diffusion coefficient given below.

1. Transport

Assuming that the diffusion process obeys the normal law $\langle r^2\rangle = 2Dt$, one may calculate the diffusion coefficient D using random walk arguments. In particular, if one neglects the time spent in a magnetized structure in the course of an interaction, the diffusion coefficient is related

to the scattering length via the usual law $D = l_{\rm scatt} c$, where the scattering length $l_{\rm scatt}$ has been defined in Eq. (8) above.

If the particle diffuses inside a structure during an interaction, then it actually gets trapped in this structure during a certain amount of time and exits backwards in a mirror-like fashion (see the appendix). Consider for simplicity a single scattering agent. One may then account for the effect of time trapping by counting the effective time taken to accomplish N steps of the random walk, which becomes $N d_i (1 + \delta t_i c/d_i)/c$. The correction decreases D by a factor $(1 + \delta t_i c/d_i)$. Since the trapping time $\delta t_i \simeq r_i/c$ is smaller than the typical distance d_i between two scattering centers, this correction is not dominant. Concerning the effect of mirroring, it suffices to note that it takes two interactions to achieve isotropic deflection; consequently, this decreases the diffusion coefficient by another factor of 2. These two corrections thus remain of order unity.

The general scaling of this diffusion coefficient with energy is easily grasped. At low energies (typically $E \lesssim 10^{18}$ eV depending on the parameters characterizing the scattering agents), it does not depend on energy, as $l_{\rm scatt}$ simply corresponds to the mean free path for scattering $\bar{d}$. In the high-energy regime, $D \propto E^2$ since the number of scatterings to achieve a deflection of order unity scales in the same way. The above diffusion coefficient may be used to describe the propagation of particles, as done in Refs. [46,95–98]. One may add that the influence of any putative all-pervading magnetic field $B_{\rm IGM}$ may be safely neglected, even at energies of order 10^{18} eV, as long as $B_{\rm IGM} \lesssim 10^{-11}$ G, since the Larmor radius $r_{\rm L} \simeq 100\ {\rm Mpc}(E/10^{18}\ {\rm eV})(B_{\rm IGM}/10^{-11}\ {\rm G})^{-1}$.

In principle, a realistic distribution of magnetic field cells inside the large scale structure might induce a scattering law with a more complex profile than the standard exponential form adopted here, which would furthermore depend on time in a nontrivial way so as to account for the effect of trapping. The particle would then follow a so-called continuous time random walk with waiting times, the properties of which can be derived by following the methods developed in Refs. [99,100]. It would certainly be particularly interesting if anomalous diffusion laws were to occur in such magnetic field configurations.

2. Experimental signatures for continuously emitting sources

The arrival direction of high-energy events will point back to the source only if this latter is located at a distance closer than $l_{\rm scatt}$. In the diffusive regime, the source distance scale is no longer $l_{\rm max}$ but $\sqrt{l_{\rm scatt} l_{\rm max}}$, since this latter gives the distance that a particle can cross before losing its energy. Since we assume $l_{\rm max} > l_{\rm scatt}$, most of the sources are located beyond $l_{\rm scatt}$.

In the steady state regime, the diffusive flux received from a source at distance l scales as $1/(l_{\rm scatt} l)$, hence, the flux received from sources within l, with $l > l_{\rm scatt}$, scales as $l^2/l_{\rm scatt}$. Consequently, the fraction of the flux that can be received from sources at distances closer than $l_{\rm scatt}$ [given by Eq. (11)] is roughly $l_{\rm scatt}/l_{\rm max}$, just as in the nondiffusive regime. This fraction gives the fraction of events behind which one can hope to detect the source.

Note that the same delusive effect of finding a scattering center in the arrival direction of cosmic rays occurs in this regime just as in the translucent regime.

On general grounds, one expects the number of multiplets to be significantly smaller in this case than for small deflection, since the angular size of the image is considerably broadened. However, sources within the sphere of large angular scattering (for which the Universe appears translucent) may produce images with higher multiplicity if they exist, i.e. if $n_{\rm s}^{-1/3} < l_{\rm scatt}$. The number of events expected from a source at distance l can be written as

$$N_{\rm m} \simeq \frac{N_{\rm obs} f_{\rm cov}}{n_{\rm s} 4\pi l^2 l_{\rm max}}. \tag{33}$$

In order to derive this estimate, it suffices to express the flux received from this source, and to replace $\dot{N}_{\rm UHECR}$ in this expression using Eq. (11). The parameter $f_{\rm cov}$ corresponds to the sensitivity of the detector in the direction of the source, normalized to the average sensitivity (i.e., on average $f_{\rm cov} = 1$). One must emphasize that the above equation assumes that all sources have the same luminosity, which may be too restrictive.

Since $N_{\rm m} \propto 1/l^2$, the maximum multiplicity N_1 will be associated to the closest source at distance $\sim n_{\rm s}^{-1/3}$

$$N_1 \simeq 0.1 f_{\rm cov} N_{\rm obs} \frac{n_{\rm s}^{-1/3}}{l_{\rm max}}. \tag{34}$$

To provide quantitative estimates, if $n_{\rm s} = n_{\rm s,-5} \times 10^{-5}\ {\rm Mpc}^{-3}$, the number of events expected from the closest source at energies greater than 4×10^{19} eV is a fraction $7 \times 10^{-3} n_{\rm s,-5}^{-1/3}$ of all observed events. This number of events becomes a fraction $0.02 n_{\rm s,-5}^{-1/3}$ of $N_{\rm obs}$ above 6×10^{19} eV.

Note that the expected multiplicity is the same in this case than that found in the absence of magnetic fields, since we assume the source to be within the sphere of large angular scattering.

3. Experimental signatures for bursting sources

As far as bursting sources such as gamma-ray bursts are concerned, most of the above results remains unchanged; one simply has to replace $n_{\rm s} \dot{N}_{\rm UHECR}$ with $\dot{n}_{\rm s} N_{\rm UHECR}$. In the present case, the typical time spread corresponds to the diffusive travel time, i.e. for a source at distance l

$$\delta t \simeq \frac{l^2}{2 l_{\rm scatt} c}. \tag{35}$$

Therefore, the number of gamma-ray bursts sources that

can contribute to the flux at a given energy E, at any time, is

$$N_{\rm GRB} \simeq \dot{n}_{\rm s} \frac{2\pi}{5} \frac{l_{\rm max}^5}{l_{\rm scatt} c}. \quad (36)$$

To make concrete estimates, at 10^{20} eV, $l_{\rm max} \simeq 95$ Mpc, hence, $N_{\rm GRB} \sim 20$ if $l_{\rm scatt} = 20$ Mpc, assuming $\dot{n}_{\rm s} = 10^{-9}$ Mpc^{-3} yr^{-1}. $N_{\rm GRB}$ is larger than unity, which implies that one should not detect significant statistical fluctuation in the energy spectrum and which explains why one can record cosmic ray events in a near continuous manner, despite the fact that close-by gamma-ray bursts are such rare events.

There will of course be an energy $E_{\rm c}$ where $l_{\rm scatt} = l_{\rm max}$, beyond which the diffusive regime will no longer apply. In this case, one must use the formulae given in Sec. III B for the translucent regime. Similarly, regarding sources located within the sphere of large angular scattering, i.e. at a distance $l < l_{\rm scatt}$, the phenomenological consequences are those described in Sec. III A if $l < \bar{d}$, or in Sec. III B if $\bar{d} < l < l_{\rm scatt}$.

IV. DISCUSSION

A. Summary of present results

The present work has provided an analytical description of ultrahigh cosmic ray transport in highly structured extragalactic magnetic fields. The corresponding configuration of the extragalactic magnetic field is that of a collection of scattering centers, such as halos of radio galaxies or starburst galaxies, or magnetized filaments, with a negligible magnetic field in between. Such a configuration is generally expected in scenarios in which the magnetic field is produced and ejected by a subclass of galaxies, or generated at the accretion shock waves of large scale structure. Even if the magnetic field is rather generated at high redshift, subsequent amplification in the shear and compressive flows of large scale structure formation tends to produce a highly structured configuration, with strong fields in the filaments of galaxies and weak fields in the voids [40,41,45,51].

In our description, transport of cosmic rays is modeled as a sequence of interactions with the scattering centers, during which the particle acquires a nonzero deflection angle and time delay (with respect to straight line crossing of the magnetized region), see the appendix. In Sec. II, we have sketched a list of possible scattering centers and their characteristics (mean free path to scattering, magnetic field, coherence length and extent). We have then computed the optical depth τ of the Universe to cosmic ray scattering as a function of energy and distance to the source, as well as the effective optical depth $\tau_{\rm eff}$ (which is defined in such a way as to become unity when the total angular deflection becomes unity). As discussed in Sec. II, the Universe can be translucent to cosmic ray scattering if $\tau > 1 > \tau_{\rm eff}$, meaning that the total deflection is smaller than unity but nonzero, opaque if $\tau > \tau_{\rm eff} > 1$, or even transparent if $1 > \tau > \tau_{\rm eff}$. For typical values of the scattering centers parameters, it is expected that the Universe be translucent or opaque on the source distance scale and at energies close to the pion production threshold. Since this energy is that generally used by experiments as a threshold for the search for counterparts, the above may have important phenomenological consequences.

In particular, in the translucent or opaque regime, the closest object lying in the cosmic ray arrival direction should be a scattering center. Since these scattering centers are sites of intense magnetic activity (radio galaxies, starburst galaxies, shock waves, ...), they might be mistaken with the source. This peculiar feature does not arise in models in which magnetic deflection is a continuous process in an all-pervading magnetic field. One could thus conceive an ''ironic'' scenario, in which cosmic rays are accelerated in gamma-ray bursts, but scatter against radio galaxies magnetized lobes, so that one interpret these latter as the source of cosmic rays, because they are the only active objects seen on the line of sight. If such counterfeiting is taking place, one should observe that the apparent distance scale to the source (actually the distance to the last scattering surface) is smaller than the expected distance scale to the source (as determined by the energy losses). This offers a simple way to test for the above effect.

In the translucent regime, the source image is broadened by an angle $\delta\alpha$, which takes values of order of a degree at energy 10^{20} eV for the fiducial values of the scattering structures that we considered: interaction length $d_i \simeq 30$ Mpc, extent $r_i \simeq 1$ Mpc, magnetic field $B \simeq 10^{-8}$ G, and coherence length $\lambda_i \simeq 0.1$ Mpc. The average optical depth at distance 100 Mpc is thus $\tau \simeq 3$ for these values. Because of the uncertainties surrounding these parameters, the deflection could, however, be larger or smaller by about an order of magnitude. In Sec. III B 2, we have discussed effects related to the shape of angular images when the discreteness of the scattering centers is taken into account.

The inhomogeneous distribution of matter in the local Universe implies that this optical depth to cosmic ray scattering should vary with the direction of observation. In Sec. III B 5, we have provided sky maps of the integrated baryonic matter density up to different distances, using the PSCz catalog of galaxies. These maps allow to estimate the fluctuation of the optical depth in different directions, hence, that of the deflection angle, since $\delta\alpha \propto \tau^{1/2}$.

In our discussion, we have taken into account the inhomogeneous distributions of the scattering centers, see Secs. II C and II D. We have shown numerically that on path lengths longer than $\sim$200 Mpc, the effect of inhomogeneity is negligible, as expected for a Universe that is homogeneous and isotropic on these scales. The path length to the first interaction is generally higher by about 40% than in the homogeneous case if the scattering centers distribute according to the dark matter density. Since scat-

tering centers tend to concentrate in filaments of large scale structure, a particle may also experience multiple interactions upon crossing a filament, as discussed and quantified in Sec. II C. This explains why the number of interactions in the inhomogeneous case converges toward that of the homogeneous case on long path lengths.

B. Recent data from the Pierre Auger observatory

In its first years of operation, the Pierre Auger Observatory has already achieved the largest aperture (in $\mathrm{km}^2 \cdot \mathrm{str} \cdot \mathrm{yr}$) [1], and it has recently released the largest catalog of events above $5.7 \cdot 10^{19}$ eV [2]. In this catalog, 20 out of 27 events originate from within 3 degrees of an active galactic nucleus located within 75 Mpc.

The most straightforward interpretation is to infer that AGN are the sources of ultrahigh energy cosmic rays. However, only one of the observed counterparts is of the FR-I type (Centaurus A), all others are more common Seyfert galaxies. From a theoretical point of view, this is unexpected, since these common AGN do not seem to offer the required characteristics for the acceleration to ultrahigh energies [101]. Even Centaurus A, as far as its jets are concerned, does not appear to be a likely source of ultrahigh energy cosmic rays [102].

Furthermore, on a purely experimental level, Gorbunov and coauthors [103] have recently pointed out an anomaly in this observed correlation. Assuming that the AGN seen in the arrival directions of these high-energy events are the source of ultrahigh energy cosmic rays, these authors have computed the expected flux using the known distances to these AGN. They have observed that the Pierre Auger Observatory has collected zero event in the direction to the Virgo cluster, whereas at least six should be expected on the basis of the large concentration of AGN in this direction and the small distance scale (assuming that the cosmic rays coming from Centaurus A indeed originate from this object).

Reference [103] thus argues that this observation rules out the possibility that AGN are the sources of ultrahigh energy cosmic rays, unless the cosmic rays seen in the direction to Centaurus A come from further away. However, as pointed out to us during the refereeing process, it could also be that the absence of AGN-like source in Virgo is a statistical fluctuation due to the small number of sources in the local Universe, or that all AGN-like sources do not have the same cosmic ray luminosity. One may also ponder on the possibility that the galactic magnetic field would exhibit a particular configuration in the direction to Virgo (which lies toward the Galactic North Pole), which would prevent cosmic rays from penetrating from this direction. Hence, at present, one cannot exclude formally that AGN are the source of ultrahigh energy cosmic rays, but the data of the Pierre Auger Observatory cannot be argued to sustend this hypothesis strongly either.

Another interpretation suggests that sources of ultrahigh energy cosmic rays cluster with the large scale structure, as AGN do; therefore, the observed correlation with AGN is a coincidence. This hypothesis deserves to be more carefully studied, for instance, by performing cross-correlations of the observed arrival directions with galaxy catalogs, or by following the method introduced in Ref. [104]. However, assuming that the sources are located close to the AGN, which have been seen in the arrival directions should not resolve the flux anomaly noted in Ref. [103], also it might mitigate it somewhat.

A third interpretation is to assume that at least part of the observed correlation is accidental because the scattering centers on the last scattering surface cluster with the large scale structure, hence, with AGN. This would alleviate this flux anomaly, since the sources would no longer have to be associated with the AGN distribution. In particular, the events seen to arise from the Centaurus complex might have been deflected in its vicinity.

As mentioned previously, this scenario can be tested by comparing the expected source distance scale with the counterpart distance scale. Interestingly, both do not match, as the source distance scale for particles with observed energy 6×10^{19} eV is of the order of 200 Mpc, significantly larger than the maximum distance of 75 Mpc for the observed counterparts. This fact has been noted in Ref. [2]; it remained mostly unexplained, although it was suggested in this work that both distance scales would agree if the energy scale were raised by 30%.

More quantitatively, one can calculate the probability that a given event with a given observed energy originates from a certain distance, using the fraction of the flux contributed by sources within a certain distance at a certain energy. This probability law can be calculated using the techniques developed in Ref. [105], then tabulated. It is then possible to calculate the probability of seeing 20 out 27 events from a source located within 75 Mpc using the events energies reported in Ref. [2]. This probability is small, about 3%; the mean lies at 15 events out of 27 coming from within 75 Mpc. If one restricts the set of events to those that lie outside the galactic plane ($|b| > 12°$), with 19 out of 21 seen to correlate, the probability becomes marginal, of order 0.1% (the mean lies at 12 out 21 within 75 Mpc). Finally, if one restricts oneself to the second set of events collected after May 27, 2006, and on those which lie outside of the galactic plane, with 9 out of 11 seen to correlate, the probability becomes of order 10%, with a mean at 7 out 11 within 75 Mpc. In this latter case, the signal is less significant, but the statistics is also smaller. Since the above estimates do not take into account the uncertainty on the energy, and since they assume continuous instead of stochastic energy losses, these numbers should be taken with caution. Nonetheless, the above estimates agree with those of Ref. [106], which indicate that 50% of protons with energy $E > 6 \times 10^{19}$ eV should come from distances less than 100 Mpc and 90% from distances less than 200 Mpc.

The above discussion suggests that, unless the energy scale is too low or an experimental artefact is present, the inferred distance scale to the source appears smaller than the expected source distance scale. In light of the analysis developed in the present paper, this suggests that part of the correlation may actually pinpoint scattering centers correlating with AGN rather than the source of ultrahigh energy cosmic rays. Said otherwise, the Pierre Auger Observatory may be seeing, at least partly, the last scattering surface of ultrahigh energy cosmic rays, rather than the source population.

In order to estimate the fraction of events that are likely to be contaminated by such pollution, one may proceed as follows. Assume first that the total deflection imparted to the particles with energy $>6\times10^{19}$ eV is less than the 3° radius used by the Pierre Auger Observatory for their search. One may then calculate the fraction of galaxies in the PSCz catalog up to a distance $l=200$ Mpc, weighted appropriately, which lies within 3° of an AGN, which is itself located closer than 75 Mpc. The distance $l=200$ Mpc is motivated by the fact that 90% of events with energy $>6\times10^{19}$ eV originate from a distance smaller than 200 Mpc [106]. One should weigh each galaxy with the selection function of the PSCz catalog at the distance l of this galaxy in order to correct for the incompleteness of the catalog; one should also weigh each galaxy with a factor $1/l^2$ to account for flux dilution during propagation. In the above estimate, the PSCz catalog is used as a tracer of the cosmic ray source population, and one simply calculates the probability of angular coincidence with the AGN sample. The number obtained is 0.31, which suggests that 31% of events above 6×10^{19} eV could correlate with the AGN, assuming that the PSCz galaxies provide an unbiased tracer of the cosmic ray source population and that the magnetic deflection is much smaller than the search radius of 3°. Note that this estimate does not take into account the effect of the magnetic field; if one were to restrict the angular radius to 2° in order to account for further possible galactic deflection, the above fraction would become 25%. For reference, the probability that a random direction on the sky falls within 3° of an AGN (located closer than 75 Mpc) is 0.22 (becoming 0.11 for a radius of 2°), which therefore gives the covering factor on the sky of these AGN.

In order to account for magnetic deflection, one may repeat the above procedure and calculate the probability of coincidence to within 3° of an AGN assuming that the event is displaced randomly by an angle $\delta\alpha$ from the location of the galaxy drawn from the PSCz catalog. Of course, one recovers the above result 0.31 for $\delta\alpha\to0$, and the probability 0.22 corresponding to isotropic source distribution for $\delta\alpha\sim1$ (in practice, $\delta\alpha\gtrsim45°$ gives a probability 0.22). Interestingly, the fraction of contaminated events increases as $\delta\alpha$ becomes of order of a few degrees: it equals 39% for $\delta\alpha=1°$, 48% for $\delta\alpha=3°$, then decreases, being 45% for $\delta\alpha=5°$ and 43% for $\delta\alpha=7°$, etc. If the radius of the correlation with the AGN is restricted to 2° to allow for further deflection in the galactic magnetic field, these numbers become 21% for $\delta\alpha=1°$, 29% for $\delta\alpha=3°$, and 25% for $\delta\alpha=5°$.

The above estimates indicate that, within the assumptions of the above discussion, the delusion should not affect all events of the Pierre Auger Observatory, but a significant fraction nonetheless, possibly as high as $\simeq50\%$. Moreover, it also indicates that intergalactic magnetic deflection could be larger than 3° and yet produce a relatively significant false correlation with AGN. If further data from cosmic ray experiments strengthen the observed correlation, then the present interpretation would fail, unless some other effects artificially enhance this false correlation.

For instance, one should point out that the above fraction of contaminated events is likely to be enhanced if ultrahigh energy cosmic rays originate from gamma-ray bursts. Indeed, as discussed in Sec. III B 5, one expects in this case the number of events in regions of low foreground density to be smaller by a factor of order τ (τ being the optical depth measured in such directions) when compared with that coming from regions of optical depth greater than unity. The main reason is that a given source has a probability $\sim\tau$ of being located behind a scattering center, which would provide sufficient time delay for the source to become observable with reasonable probability. On the contrary, a nearby gamma-ray burst with no scattering center on the line of sight has a negligible probability of being seen during a time span of a few years as a result of the small occurrence rate. Although it is difficult to give a simple estimate of the magnitude of this effect on the amount of false correlations, one can easily see that it would tend to increase this fraction by providing more weight to regions of high foreground density (in which AGN are more numerous).

In Ref. [2], the Pierre Auger Observatory has discussed the evolution of the probability of null hypothesis for an isotropic distribution of sources with a varying search radius, maximum AGN redshift and minimum energy (see Fig. 3 of Ref. [2]). The minimum probability (which indicates a maximal correlation with the AGN) corresponds to a search radius 3.2°. This minimum can be interpreted as an estimate of the amount of galactic and intergalactic magnetic deflection, if one assumes that the source exactly correlates with the AGN. Interestingly, our above discussion suggests that this number may be a biased estimate and that the intergalactic deflection could be slightly larger. The increase of the probability of null hypothesis at larger search radii in the Pierre Auger data corresponds to the fact that the covering factor of the search area increases rapidly with search radius, being already 0.50 at 6°. Concerning the redshift evolution, one would expect in the present model that the correlation would persist to distances as large as 200 Mpc, if the search

radius is larger than the typical intergalactic deflection. Unfortunately, Ref. [2] does not plot this correlation beyond 100 Mpc. It would be interesting to also carry out this test for different search radii.

One should emphasize that in the present interpretation, the correlation with AGN should not persist as the threshold energy is decreased. Indeed, the maximum propagation distance of particles of observed energy 4×10^{19} eV is of order 500 Mpc, on which scale the Universe appears isotropic. Therefore, at these energies the incoming flux is increasingly isotropic, and the presence of scattering centers on the line of sight cannot induce anisotropies on an isotropic sky distribution (see discussion in Sec. III B 2 as well as the discussion on the application of the Liouville theorem in Ref. [94]). The fraction of flux contributed by the isotropic background has been estimated in Ref. [107] in the absence of extragalactic magnetic field; it reaches 83% for $E > 3 \times 10^{19}$ eV, and 3.6% for $E > 5 \times 10^{19}$ eV. The strong rise toward isotropy as the threshold energy decreases is thus clear. This effect is present, at least qualitatively, in the data of the Pierre Auger Observatory (see Fig. 3 of Ref. [2]).

Finally, it appears that comparing the apparent source distance scale with the expected one, as we have done above, remains the most direct and simple test of the present interpretation. Since there is a non-negligible degeneracy between the expected distance scale and the energy calibration, it seems mandatory to obtain a calibration through other methods that is as accurate as possible.

It also appears imperative to probe the arrival directions on an event by event basis, focussing on the most energetic events. In the catalog reported in Ref. [2], there is only one event above 10^{20} eV, whose arrival direction has a relatively small supergalactic latitude $b_{\rm SG} \simeq -6.5°$. In the above scenario, one should expect to find a scattering center or the source on the line of sight; hence, it should prove useful to perform a deep search in this direction in the radio domain, looking for traces of synchrotron emission that would attest of the presence of a locally enhanced intergalactic magnetic field. Many more events at higher energies, as expected from future detectors such as Auger North [108], would certainly help in this regard.

A last word should be added concerning the amount of magnetic deflection and the source models. In particular, it would be interesting to examine whether (and to what cost) the current data could be reconciled with ultrahigh energy cosmic rays being accelerated in the most powerful AGN, which offer stronger ground than Seyfert galaxies for acceleration. Such a study can only be conducted through detailed Monte Carlo simulations, which allow for substantial scattering angles in inhomogeneous magnetic fields.

As explained in Ref. [91], gamma-ray bursts are probably the most elusive of possible ultrahigh energy cosmic ray sources, as the strongest predictions are that no counterpart should be detected, that the flux should show significant variations around the mean at sufficiently high energies (a few 10^{20} eV), and that multiplets of events should be clustered in energy. Current data do not violate any of these predictions, but it is clear that experiments with much larger aperture at the highest energies will be needed to test such effects.

It is certain that much physics and astrophysics of cosmic ray sources and large scale magnetic fields remain to be unveiled by ongoing and future detectors.

ACKNOWLEDGMENTS

We thank S. Colombi for providing the dark matter simulation and H. Atek, G. Boué, N. Busca, Y. Dubois, E. Hivon, A. Olinto, C. Pichon, and S. Prunet for discussions.

APPENDIX: PARTICLE—SCATTERING CENTER INTERACTION

This section describes the interaction between a particle and a scattering center in the large scale structure, then computes the deflection angle and the trapping time in the structure before its return to nonmagnetized voids. We consider both the cylindrical geometry, which is representative of an interaction with a filament, and the spherical geometry, which we use to model the interaction with a magnetized wind or cocoon. The solution of the diffusion equation in a planar geometry can be found in Ref. [90].

This discussion assumes that the magnetic field strength and the diffusion coefficient are uniform in the scattering center. Expectations in the more general nonuniform case are discussed briefly at the end of this appendix.

1. Interaction with a sphere or a filament: General results

If the scattering length $l_{\rm sc}$ of the particle in the scattering center is much larger than the characteristic path length $\bar{r}_i$ through the structure, the particle is simply deflected by an angle $\delta\theta_i$ and emerges after a crossing time $t \simeq \bar{r}_i/c$. The characteristic size $\bar{r}_i$ should be thought of as the smallest length scale of the structure, i.e. $(\pi/2)r_{\rm s}$ for a sphere or $(\pi/2)^2 r_{\rm f}$ for a filament. The factors of $\pi/2$ account for random orientation of the incoming direction.

The deflection angle at each interaction can be computed as follows. Consider a spherical magnetized halo of radius r_i, magnetic field B_i, and magnetic coherence length λ_i. The magnetic scattering length $l_{\rm sc}$ of a particle of Larmor radius $r_{\rm L}$ in this structure determines the length beyond which the particle has experienced a deflection of order unity. Hence, if $l_{\rm sc} \ll r_i$, the particle undergoes diffusion in the structure so that $\delta\theta_i \sim \mathcal{O}(1)$. In the following section, it is also shown that the distance traveled in the structure is very small as compared with r_i, so that escape actually takes place close to the point of entry with a mirrorlike deflection of order π (to within $\pm\pi/2$).

If, however, $l_{\rm sc} \gg r_i$, the particle is only weakly deflected. In order to calculate $\delta\theta_i^2$, one must specify $l_{\rm sc}$ as a function of $r_{\rm L}$ and λ_i. The general relationship between these quantities can be expressed as

$$l_{\rm sc} \simeq \alpha r_{\rm L}\left(\frac{r_{\rm L}}{\lambda_i}\right)^{\beta}. \tag{A1}$$

This equation neglects a numerical prefactor of order unity (see Ref. [102] for more details). The coefficient α is directly related to the level of turbulence in the structure

$$\alpha = \left(\frac{\delta B_i^2}{B_i^2}\right)^{-1}, \tag{A2}$$

where δB_i represents the turbulent component and B_i the total magnetic field. In the following, we assume $\alpha \simeq 1$, meaning full turbulence, but the calculations that follow may be generalized to $\alpha \neq 1$ without difficulty. The various scenarios of magnetic pollution discussed before do not favor the existence of significant coherent components of the magnetic field.

Regarding the exponent β, $\beta = 1$ if $r_{\rm L} \gg \lambda_i$ [102,109,110]. If, however, $r_{\rm L} \ll \lambda_i$, then β also depends on the shape of the turbulence spectrum. For instance, $\beta = -2/3$ for Kolmogorov turbulence, $\beta = 0$ for scale invariant turbulence (Bohm regime). For simplicity, and in the absence of any knowledge of the turbulence spectrum in the scattering centers, we assume $\beta = 0$, which allows to simplify the discussion. Again, it is possible to extend the discussion to different values of β, albeit at the price of slightly more complicated expressions.

Therefore, one finds the following deflection angle. If $r_{\rm L} \ll \lambda_i$, then $l_{\rm sc} \simeq r_{\rm L} \ll \lambda_i < r_i$; hence, the particle diffuses in the structure and exits with a deflection of order unity. Note that the inequality $\lambda_i < r_i$ simply states that the coherence length of the magnetic field cannot exceed the size of the magnetic structure.

If $r_{\rm L} \gg \lambda_i$, then $l_{\rm sc} \simeq r_{\rm L}^2/\lambda_i$. One then must consider whether $r_{\rm L}$ is larger or smaller than $\sqrt{\lambda_i r_i}$. In the former case, $l_{\rm sc} \gg r_i$; hence, the particle exits with a small deflection angle $\delta\theta_i^2 \simeq \bar{r}_i\lambda_i/(2r_{\rm L}^2)$ [16]. This numerical prefactor $1/2$ is valid for propagation in a turbulent magnetic field; it becomes $2/3$ for a randomly oriented regular magnetic field [14].

In the latter case, $l_{\rm sc} \ll r_i$; hence, the particle exits with a deflection angle of order unity.

In conclusion, the deflection angle can be written in the approximate form

$$\delta\theta_i^2 \simeq \left(1 + \frac{2r_{\rm L}^2}{\bar{r}_i\lambda_i}\right)^{-1}. \tag{A3}$$

Although this form is only approximate, it interpolates smoothly between the two different regimes of interest $r_{\rm L} \ll \sqrt{r_i\lambda_i}$ (large deflection) and $r_{\rm L} \gg \sqrt{r_i\lambda_i}$ (small deflection). In the high-energy (small deflection) limit, one finds

$$\delta\theta_i \simeq 1.7^\circ\left(\frac{\bar{r}_i}{2\ {\rm Mpc}}\right)^{1/2}\left(\frac{B_i}{10^{-8}\ {\rm G}}\right)\left(\frac{\lambda_i}{0.1\ {\rm Mpc}}\right)^{1/2} \times \left(\frac{E}{10^{20}\ {\rm eV}}\right)^{-1}. \tag{A4}$$

The time delay with respect to straight line crossing of the magnetized structure can be calculated, following Refs. [14,16,89]

$$\delta t_i \simeq \frac{\bar{r}_i\delta\theta_i^2}{6c}. \tag{A5}$$

This formula is only valid for small deflection angles; the corresponding time delay in the diffusive regime is discussed further below. In the high-energy limit $r_{\rm L} \gg \sqrt{r_i\lambda_i}$, this gives

$$\delta t_i \simeq 0.93 \times 10^3\ {\rm yr}\left(\frac{\bar{r}_i}{2\ {\rm Mpc}}\right)^2\left(\frac{B_i}{10^{-8}\ {\rm G}}\right)^2\left(\frac{\lambda_i}{0.1\ {\rm Mpc}}\right) \times \left(\frac{E}{10^{20}\ {\rm eV}}\right)^{-2}. \tag{A6}$$

2. Diffusive interaction with a filament

If $l_{\rm sc} \ll r_{\rm f}$, the particle diffuses inside the filament before escaping. One can assume that the particle penetrates a length scale $l_{\rm sc}$ inside the filament, and then enters the diffusive regime. The time-dependent diffusion equation can then be used to compute the probability of escape as a function of time, treating the point of first interaction (at depth $l_{\rm sc}$) as an impulsive source. To this effect, we describe the filament as a cylinder of radius $r_{\rm f}$ and infinite extension along z and consider cylindrical coordinates (r, θ, z). For simplicity, we assume a spatially uniform diffusion coefficient $D_\perp$ in the plane perpendicular to z, and a spatially uniform diffusion coefficient $D_\parallel$ in the direction along z. We also neglect energy losses, which is justified in so far as we will show that the trapping time is short on the typical energy loss time scale. The equation for the Green's function $g(r, \theta, z, t; r_0, \theta_0, z_0, t_0)$ reads

$$\partial_t g - D_\perp\frac{1}{r}\partial_r(r\partial_r g) - D_\perp\frac{1}{r^2}\partial_\theta^2 g - D_\parallel\partial_z^2 g = \frac{1}{r}\delta(z - z_0)\delta(r - r_0)\delta(\theta - \theta_0)\delta(t - t_0). \tag{A7}$$

Here, r_0, θ_0, z_0 and t_0 give the coordinates of the first interaction in the filament. One must also take into account the appropriate boundary conditions, namely, that beyond radius $r_{\rm f}$, the volume is unmagnetized. In the theory of diffusion, such boundary conditions can be modeled by ensuring that the solution to the diffusion equation vanishes at a radius $r_{\rm f}$. In order to solve the diffusion equation in cylindrical coordinates under this constraint, one expands the angular part of the Green's function g over a basis of proper functions of the operator ∂_θ^2 and the radial part over a basis of Bessel functions $J_m(\alpha_{ms}r/r_{\rm f})$, where α_{ms} de-

notes the s-th root of J_m. This guarantees that the boundary condition will be satisfied. The solution of Eq. (A7) reads

$$g(r,\theta,z,t;r_0,\theta_0,z_0,t_0) = \frac{1}{\pi r_f^2}\sum_{m=-\infty}^{m=+\infty}\sum_{s=1}^{s=+\infty} e^{im(\theta-\theta_0)} \times e^{-\alpha_{ms}^2 D_\perp |t-t_0|/r_f^2} \times \frac{e^{-|z-z_0|^2/4D_\parallel|t-t_0|}}{\sqrt{4\pi D_\parallel |t-t_0|}} \times \frac{J_m(\alpha_{ms}\frac{r_0}{r_f})J_m(\alpha_{ms}\frac{r}{r_f})}{J_{m+1}(\alpha_{ms})^2}. \quad \text{(A8)}$$

The probability of having the particle inside the filament at any time $t > t_0$ is then given by the volume average of g over the filament

$$P_{\rm res}(t;t_0) = \int \mathrm{d}v g = \sum_{s=1}^{s=+\infty} e^{-\alpha_{0s}^2 D_\perp |t-t_0|/r_f^2}\frac{2}{\alpha_{0s}}\frac{J_0(\alpha_{0s}\frac{r_0}{r_f})}{J_1(\alpha_{0s})}. \quad \text{(A9)}$$

Through the explicit decomposition of unity over the above basis of Bessel functions, one can verify that $P_{\rm esc}(t\to t_0) = 1$ as it should. The form of $P_{\rm res}(t;t_0)$ tends to suggest that escape takes place on a diffusive time scale $r_f^2/D_\perp$; this statement is actually too naive, as shown in the following. The average residence time in the filament δt_f is calculated as

$$\delta t_f = \int_{t_0}^{+\infty} \mathrm{d}t P_{\rm res}(t;t_0) = \frac{r_f^2}{2D_\perp}\sum_{s=1}^{s=+\infty}\frac{4}{\alpha_{0s}^3}\frac{J_0(\alpha_{0s}\frac{r_0}{r_f})}{J_1(\alpha_{0s})}. \quad \text{(A10)}$$

The factors in the sum on the right-hand side. of Eq. (A10) are much smaller than unity because the particle cannot penetrate further than $l_{sc} \ll r_f$ into the filament before starting to diffuse; hence, $r_0 \simeq r_f(1 - l_{sc}/r_f)$. This substitution followed by the expansion of the Bessel functions to first order in terms of l_{sc}/r_f leads to the trapping time

$$\delta t_f \simeq \frac{r_f l_{sc}}{D_\perp}\sum_{s=1}^{s=+\infty}\frac{2}{\alpha_{0s}^2}, \quad \text{(A11)}$$

which is effectively smaller than the diffusive time by a factor l_{sc}/r_f. Since $D_\perp = \frac{1}{2} l_{sc} c$, one finally obtains

$$\delta t_f \simeq \frac{r_f}{c}\sum_{s=1}^{s=+\infty}\frac{4}{\alpha_{0s}^2} = \frac{r_f}{c}. \quad \text{(A12)}$$

Alternatively, one could calculate the residence time by averaging Eq. (A10) over the probability of first scattering $P(r_0) \simeq \exp[-(r_f - r_0)/l_{sc}]/l_{sc}$, but this would lead to similar results.

We thus find that the trapping time is of order of the crossing time, an unexpected result. Since the particle diffuses, the linear length scale traveled in this trapping time is only $l \sim (l_{sc}/r_f)^{1/2} r_f \ll r_f$. Hence, the particle enters and exits the filament at about the same location, albeit a crossing time later. In terms of angular scattering, this interaction is thus akin to mirroring, as the particle will exit in a direction separated by less than $\pi/2$ from the direction of entry in the filament.

This law $\delta t_f \simeq r_f/c$ has been verified numerically, using Monte Carlo simulations of the interaction of a particle with a magnetized filament, for various coherence lengths of the magnetic field. The numerical code used has been described in detail in Ref. [46]. The results are shown in Fig. 9 below, where it is seen that the average residence time does not depend on the coherence length of the magnetic field (which characterizes the diffusion coefficient, hence, the scattering length), but evolves linearly with the filament radius. Numerically, one obtains $\delta t_f \simeq 1.3 r_f/c$.

3. Diffusive interaction with a sphere

The interaction with a sphere of radius r_s is quite similar to that with a filament, although the algebra is slightly more cumbersome. As before, we assume that the particle penetrates a length scale l_{sc} before starting to diffuse in the magnetized sphere, and adopt appropriate boundary conditions at radius r_s. The diffusion equation in spherical

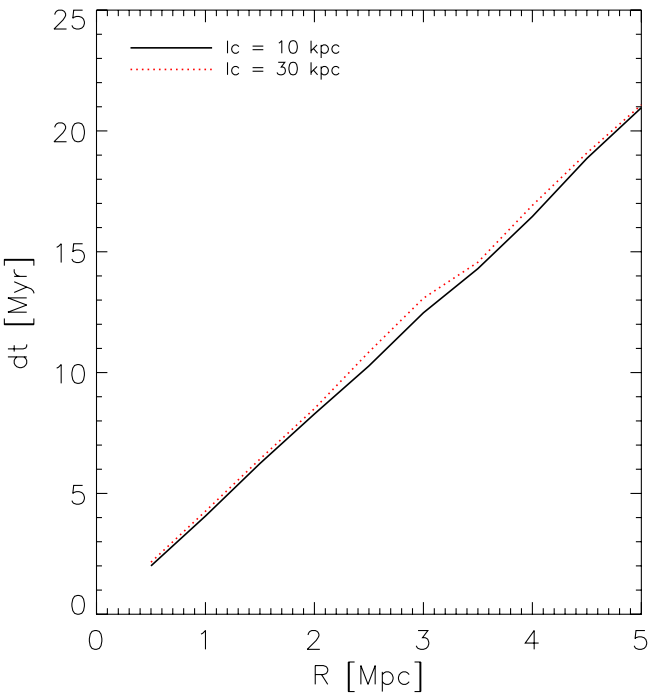

FIG. 9 (color online). Residence time in a magnetized filament embedded in a nonmagnetized medium for a particle impinging on the filament with a scattering length $l_{sc} \ll r_f$, as a function of the radius of the filament. The scattering length is a function of the coherence length of the magnetic field λ, that corresponds to the modelling of Kolmogorov turbulence inside the filament, i.e. $l_{sc} \propto \lambda^{2/3}$, see Ref. [46].

coordinates reads

$$\partial_t g - \frac{D}{r^2}\partial_r(r^2\partial_r g) - \frac{D}{r^2\sin\theta}\partial_\theta(\sin\theta\partial_\theta g) - \frac{D}{r^2\sin^2\theta}\partial_\phi^2 g = \frac{1}{r^2\sin\theta}\delta(r-r_0)\delta(\theta-\theta_0)\delta(\phi-\phi_0)\delta(t-t_0). \tag{A13}$$

Its solution is written in terms of spherical harmonics and spherical Bessel functions

$$g(r,\theta,\phi,t;r_0,\theta_0,\phi_0,t_0) = \sum_{l=0}^{l=+\infty}\sum_{m=-l}^{m=+l}\sum_{s=1}^{s=+\infty} e^{-\beta_{ls}^2 D|t-t_0|/r_s^2} \times Y_{lm}(\theta,\phi)\bar{Y}_{lm}(\theta_0,\phi_0) \times j_l\left(\beta_{ls}\frac{r}{r_s}\right)j_l\left(\beta_{ls}\frac{r_0}{r_s}\right) \times \frac{2}{r_s^3 j_{l+1}^2(\beta_{ls})}. \tag{A14}$$

The notation β_{ls} indicates the s-th zero of the spherical Bessel function j_l. As before, the probability of residence inside the spherical structure at time $t > t_0$ can be computed by integrating g over the volume

$$P_{\rm res}(t;t_0) = \sum_{s=1}^{s=+\infty} e^{-\beta_{0s}^2 D|t-t_0|/r_s^2} j_0\left(\beta_{0s}\frac{r_0}{r_s}\right)\frac{2}{\beta_{0s}j_1(\beta_{0s})}. \tag{A15}$$

Here as well, $P_{\rm res}(t\to t_0) = 1$ as it should. Finally, the residence time can be calculated by taking the limit $r_0 \to r_s(1 - l_{\rm sc}/r_s)$ as before and expanding to first order in $l_{\rm sc}/r_s$

$$\delta t_s = \int_{t_0}^{+\infty} {\rm d}t P_{\rm res}(t;t_0) \simeq \frac{r_s}{c}\sum_{s=1}^{s=+\infty}\frac{6}{\beta_{0s}^2} = \frac{r_s}{c}. \tag{A16}$$

The particle bounces on the sphere, exiting at a distance $l \sim (l_{\rm sc}/r_s)^{1/2} r_s \ll r_s$ away from its point of impact.

4. Nonuniform magnetic field

The above discussion has assumed that the magnetic field and the diffusion coefficient are uniform in the scattering center. If the length scale of variation of the magnetic field, $l_B = |\nabla B^2/B^2|^{-1}$ is "small enough," the discussion becomes more intricate as the scattering length of the cosmic ray becomes itself space dependent, and meaningless if it is larger than l_B. Nevertheless, one may expect the following to occur.

If the scattering length as measured everywhere in the scattering center is larger than its size r, then the total deflection will remain much smaller than unity. Its value will be given by an average of order $\langle r l_B/r_{\rm L}^2\rangle$, where the average is to be taken on $r_{\rm L}$ (through its spatial dependence via B) on the trajectory. This estimate assumes that the particle is deflected by $\delta\theta^2 \sim (l_B/r_{\rm L})^2$ every l_B. Its corresponds to the estimate of the above discussion if λ is replaced by l_B and if B is understood as the average magnetic field. The crossing time will remain unchanged, of order r/c.

If the scattering length is everywhere smaller than r, then the above results should not be modified, i.e. the particle will bounce on the scattering center with a trapping time of order r/c.

Consider now the intermediate case, for instance, that where the scattering center has a core with a magnetic field such that $l_{\rm sc}$ becomes smaller than the size of the core $r_{\rm c}$, surrounded by an envelope with B such that $l_{\rm sc} \gtrsim r$. With probability $\sim(r_{\rm c}/r)^2$, the particle may cross the envelope and bounce on the core; in this case the deflection angle is of order unity and the total crossing time of order r/c. With probability $\sim 1 - (r_{\rm c}/r)^2$, the particle may also cross the envelope without interacting with the core and suffer a deflection smaller than unity as calculated above; the crossing time remains the same. The typical deflection angle over many interactions of for many particles is of course given by the average of these two possibilities.

[1] J. Abraham *et al.* (The Pierre Auger Collaboration), Science **318**, 938 (2007).
[2] J. Abraham *et al.* (The Pierre Auger Collaboration) Astropart. Phys. **29**,188 (2008).
[3] T. Stanev, P. L. Biermann, J. Lloyd-Evans, J. P. Rachen, and A. A. Watson, Phys. Rev. Lett. **75**, 3056 (1995).
[4] P. G. Tinyakov and I. I. Tkachev, JETP Lett. **74**, 445 (2001).
[5] D. S. Gorbunov, P. G. Tinyakov, I. I. Tkachev, and S. V. Troitsky, JETP Lett. **80**, 145 (2004); Pisma Zh. Eksp. Teor. Fiz. **80**, 167 (2004).
[6] P. G. Tinyakov and I. I. Tkachev, Phys. Rev. D **69**, 128301 (2004).
[7] N. W. Evans, F. Ferrer, and S. Sarkar, Phys. Rev. D **69**, 128302 (2004).
[8] R. U. Abbasi, T. Abu-Zayyad, J. F. Amann, G. Archbold, K. Belov, J. W. Belz, S. BenZvi, D. R. Bergman, S. A. Blake, and J. H. Boyer *et al.*, Astrophys. J. **636**, 680 (2006).
[9] Y. Uchihori, M. Nagano, M. Takeda, M. Teshima, J. Lloyd-Evans, and A. A. Watson, Astropart. Phys. **13**, 151 (2000).
[10] G. R. Farrar, A. A. Berlind, and D. W. Hogg, Astrophys. J. Lett. **642**, L89 (2006).
[11] R. U. Abbasi, T. Abu-Zayyad, J. F. Amann, G. Archbold, R. Atkins, J. A. Bellido, K. Belov, J. W. Belz, S. Y. Ben-

Zvi, and D. R. Bergman *et al.*, Astrophys. J. **623**, 164 (2005).
[12] P. P. Kronberg, Rep. Prog. Phys. **57**, 325 (1994).
[13] J. P. Vallée, Fundam. Cosm. Phys. **19**, 1 (1997).
[14] E. Waxman and J. Miralda-Escudé, Astrophys. J. **472**, L89 (1996).
[15] A. Achterberg, Y. A. Gallant, C. A. Norman, and D. B. Melrose, arXiv:astro-ph/9907060 [Astrophysics (Engl. Transl.) (to be published)].
[16] D. Harari, S. Mollerach, E. Roulet, and F. Sánchez, J. High Energy Phys. 3 (2002) 45.
[17] D. Harari, S. Mollerach, and E. Roulet, J. High Energy Phys. 7 (2002) 6.
[18] J. Wdowczyk and A. W. Wolfendale, Nature (London) **281**, 356 (1979).
[19] V. S. Berezinskii, S. I. Grigor'eva, and V. A. Dogiel, Astron. Astrophys. **232**, 582 (1990).
[20] P. Blasi and A. V. Olinto, Phys. Rev. D **59**, 023001 (1998).
[21] R. Lampard, R. W. Clay, and B. R. Dawson, Astropart. Phys. **7**, 213 (1997).
[22] G. A. Medina Tanco, E. M. de Gouveia dal Pino, and J. E. Horvath, Astropart. Phys. **6**, 337 (1997).
[23] M. Lemoine, G. Sigl, A. Olinto, and D. N. Schramm, Astrophys. J. **486**, L115 (1997).
[24] G. Sigl, M. Lemoine, and A. V. Olinto, Phys. Rev. D **56**, 4470 (1997).
[25] R. W. Clay, S. Cook, B. R. Dawson, A. G. K. Smith, and R. Lampard, Astropart. Phys. **9**, 221 (1998).
[26] T. Stanev, R. Engel, A. Mücke, R. J. Protheroe, and J. P. Rachen, Phys. Rev. D **62**, 093005 (2000).
[27] H. Yoshiguchi, S. Nagataki, S.-y. Tsubaki, and K. Sato, Astrophys. J. **586**, 1211 (2003).
[28] O. Deligny, A. Letessier-Selvon, and E. Parizot, Astropart. Phys. **21**, 609 (2004).
[29] G. A. Medina Tanco, Astrophys. J. Lett. **505**, L79 (1998).
[30] G. Sigl, M. Lemoine, and P. Biermann, Astropart. Phys. **10**, 141 (1999).
[31] M. Lemoine, G. Sigl, and P. Biermann, arXiv:astro-ph/9903124.
[32] Y. Ide, S. Nagataki, S. Tsubaki, H. Yoshiguchi, and K. Sato, Publ. Astron. Soc. Jpn. **53**, 1153 (2001).
[33] C. Isola, M. Lemoine, and G. Sigl, Phys. Rev. D **65**, 023004 (2001).
[34] C. Isola and G. Sigl, Phys. Rev. D **66**, 083002 (2002).
[35] T. Stanev, D. Seckel, and R. Engel, Phys. Rev. D **68**, 103004 (2003).
[36] G. Sigl, F. Miniati, and T. A. Enßlin, Phys. Rev. D **68**, 043002 (2003).
[37] G. Sigl, F. Miniati, and T. A. Enßlin, Phys. Rev. D **70**, 043007 (2004).
[38] E. Armengaud, G. Sigl, and F. Miniati, Phys. Rev. D **72**, 043009 (2005).
[39] K. Dolag, D. Grasso, V. Springel, and I. Tkachev, J. Korean Astron. Soc. **37**, 427 (2004).
[40] K. Dolag, D. Grasso, V. Springel, and I. Tkachev, J. Cosmol. Astropart. Phys. 1 (2005) 9.
[41] H. Kang, S. Das, D. Ryu, and J. Cho, arXiv:0706.2597.
[42] G. Sigl, Phys. Rev. D **75**, 103001 (2007).
[43] G. A. Medina Tanco, arXiv:astro-ph/9707054.
[44] H. Takami, H. Yoshiguchi, and K. Sato, Astrophys. J. **639**, 803 (2006).
[45] H. Takami and K. Sato, arXiv:0706.3666.
[46] K. Kotera and M. Lemoine, Phys. Rev. D **77**, 023005 (2008).
[47] G. Medina-Tanco and T. A. Enßlin, Astropart. Phys. **16**, 47 (2001).
[48] V. Berezinsky, A. Z. Gazizov, and S. I. Grigorieva, arXiv: astro-ph/0210095.
[49] L. M. Widrow, Rev. Mod. Phys. **74**, 775 (2002).
[50] D. Ryu, H. Kang, and P. L. Biermann, Astron. Astrophys. **335**, 19 (1998).
[51] G. Sigl, F. Miniati, and T. A. Enßlin, Phys. Rev. D **70**, 043007 (2004).
[52] K. Dolag, Astron. Nachr. **327**, 575 (2006).
[53] P. P. Kronberg, H. Lesch, and U. Hopp, Astrophys. J. **511**, 56 (1999).
[54] G. T. Birk, H. Wiechen, H. Lesch, and P. P. Kronberg, Astron. Astrophys. **353**, 108 (2000).
[55] S. Bertone, C. Vogt, and T. Enßlin, Mon. Not. R. Astron. Soc. **370**, 319 (2006).
[56] M. J. Rees and G. Setti, Nature (London) **219**, 127 (1968).
[57] S. R. Furlanetto and A. Loeb, Astrophys. J. **556**, 619 (2001).
[58] Gopal-Krishna and P. J. Wiita, Astrophys. J. Lett. **560**, L115 (2001).
[59] S. Bertone, F. Stoehr, and S. D. M. White, Mon. Not. R. Astron. Soc. **359**, 1201 (2005).
[60] P. P. Kronberg, Q. W. Dufton, H. Li, and S. A. Colgate, Astrophys. J. **560**, 178 (2001).
[61] L. Ferrarese and H. Ford, Space Sci. Rev. **116**, 523 (2005).
[62] T. R. Lauer, S. M. Faber, D. Richstone, K. Gebhardt, S. Tremaine, M. Postman, A. Dressler, M. C. Aller, A. V. Filippenko, and R. Green *et al.*, Astrophys. J. **662**, 808 (2007).
[63] E. R. Seaquist and N. Odegard, Astrophys. J. **369**, 320 (1991).
[64] M. Pettini, S. A. Rix, C. C. Steidel, K. L. Adelberger, M. P. Hunt, and A. E. Shapley, Astrophys. J. **569**, 742 (2002).
[65] K. L. Adelberger, C. C. Steidel, A. E. Shapley, and M. Pettini, Astrophys. J. **584**, 45 (2003).
[66] T. M. Heckman, in *Gas and Galaxy Evolution*, Astronomical Society of the Pacific Conference Series Vol. 240, edited by J. E. Hibbard, M. Rupen, and J. H. van Gorkom, (Astronomical Society of the Pacific, San Francisco, 2001), p. 345.
[67] A. Aguirre, L. Hernquist, J. Schaye, D. H. Weinberg, N. Katz, and J. Gardner, Astrophys. J. **560**, 599 (2001).
[68] R. Cen, K. Nagamine, and J. P. Ostriker, Astrophys. J. **635**, 86 (2005).
[69] E. Scannapieco, C. Pichon, B. Aracil, P. Petitjean, R. J. Thacker, D. Pogosyan, J. Bergeron, and H. M. P. Couchman, Mon. Not. R. Astron. Soc. **365**, 615 (2006).
[70] H.-P. Reuter, U. Klein, H. Lesch, R. Wielebinski, and P. P. Kronberg, Astron. Astrophys. **256**, 10 (1992).
[71] T. E. Clarke, P. P. Kronberg, and H. Böhringer, Astrophys. J. Lett. **547**, L111 (2001).
[72] F. Govoni, M. Murgia, L. Feretti, G. Giovannini, K. Dolag, and G. B. Taylor, Astron. Astrophys. **460**, 425 (2006).
[73] M. Brüggen, M. Ruszkowski, A. Simionescu, M. Hoeft, and C. Dalla Vecchia, Astrophys. J. Lett. **631**, L21 (2005).

[74] A. G. Doroshkevich, D. L. Tucker, R. Fong, V. Turchaninov, and H. Lin, Mon. Not. R. Astron. Soc. **322**, 369 (2001).
[75] F. Miniati, D. Ryu, H. Kang, T. W. Jones, R. Cen, and J. P. Ostriker, Astrophys. J. **542**, 608 (2000).
[76] H. Kang, D. Ryu, R. Cen, and D. Song, Astrophys. J. **620**, 21 (2005).
[77] R. M. Kulsrud, R. Cen, J. P. Ostriker, and D. Ryu, Astrophys. J. **480**, 481 (1997).
[78] A. Loeb and E. Waxman, Nature (London) **405**, 156 (2000).
[79] F. Miniati, Mon. Not. R. Astron. Soc. **337**, 199 (2002).
[80] U. Keshet, E. Waxman, A. Loeb, V. Springel, and L. Hernquist, Astrophys. J. **585**, 128 (2003).
[81] J. Vink and J. M. Laming, Astrophys. J. **584**, 758 (2003).
[82] E. G. Berezhko, L. T. Ksenofontov, and H. J. Völk, Astron. Astrophys. **412**, L11 (2003).
[83] K. Greisen, Phys. Rev. Lett. **16**, 748 (1966).
[84] G. T. Zatsepin and V. A. Kuzmin, JETP Lett. **4**, 78 (1966).
[85] R. Teyssier, Astron. Astrophys. **385**, 337 (2002).
[86] E. Waxman, Phys. Rev. Lett. **75**, 386 (1995).
[87] J. Alvarez-Muñiz, R. Engel, and T. Stanev, Astrophys. J. **572**, 185 (2002).
[88] H. Takami and K. Sato, arXiv:0711.2386.
[89] C. Alcock and S. Hatchett, Astrophys. J. **222**, 456 (1978).
[90] G. Sigl, M. Lemoine, and P. Biermann, Astropart. Phys. **10**, 141 (1999).
[91] E. Waxman, in *Physics and Astrophysics of Ultra-High-Energy Cosmic Rays*, edited by M. Lemoine and G. Sigl, Lecture Notes in Physics Vol. 576 (Springer Verlag, Berlin, 2001), p. 122.
[92] W. Saunders, W. J. Sutherland, S. J. Maddox, O. Keeble, S. J. Oliver, M. Rowan-Robinson, R. G. McMahon, G. P. Efstathiou, H. Tadros, and S. D. M. White *et al.*, Mon. Not. R. Astron. Soc. **317**, 55 (2000).
[93] K. M. Górski, E. Hivon, A. J. Banday, B. D. Wandelt, F. K. Hansen, M. Reinecke, and M. Bartelmann, Astrophys. J. **622**, 759 (2005).
[94] D. Harari, S. Mollerach, and E. Roulet, J. High Energy Phys. 8 (1999) 22.
[95] R. Aloisio and V. Berezinsky, Astrophys. J. **612**, 900 (2004).
[96] V. Berezinsky and A. Gazizov, Astrophys. J. **643**, 8 (2006).
[97] M. Lemoine, Phys. Rev. D **71**, 083007 (2005).
[98] R. Aloisio and V. Berezinsky, Astrophys. J. **625**, 249 (2005).
[99] J.-P. Bouchaud and A. Georges, Phys. Rep. **195**, 127 (1990).
[100] R. C. Ball, S. Havlin, and G. H. Weiss, J. Phys. A **20**, 4055 (1987).
[101] C. A. Norman, D. B. Melrose, and A. Achterberg, Astrophys. J. **454**, 60 (1995).
[102] F. Casse, M. Lemoine, and G. Pelletier, Phys. Rev. D **65**, 023002 (2001).
[103] D. Gorbunov, P. Tinyakov, I. Tkachev, and S. Troitsky, arXiv:0711.4060.
[104] E. Waxman, K. B. Fisher, and T. Piran, Astrophys. J. **483**, 1 (1997).
[105] V. Berezinsky, A. Gazizov, and S. Grigorieva, Phys. Rev. D **74**, 043005 (2006).
[106] D. Harari, S. Mollerach, and E. Roulet, J. Cosmol. Astropart. Phys. 11 (2006) 12.
[107] A. Cuoco, R. D'Abrusco, G. Longo, G. Miele, and P. D. Serpico, J. Cosmol. Astropart. Phys. 1 (2006) 9.
[108] Pierre Auger North Observatory, http://www.augernorth.org.
[109] J. Giacalone and J. R. Jokipii, Astrophys. J. **520**, 204 (1999).
[110] J. Candia and E. Roulet, J. Cosmol. Astropart. Phys. 10 (2004) 007.